The Astrophysical Journal Supplement Series, 183:1–16, 2009 July doi:10.1088/0067-0049/183/1/1

A SEARCH FOR "DWARF" SEYFERT NUCLEI. VII. A CATALOG OF CENTRAL STELLAR VELOCITY DISPERSIONS OF NEARBY GALAXIES

Luis C. Ho[1], Jenny E. Greene[2,5], Alexei V. Filippenko[3], and Wallace L. W. Sargent[4]
[1] The Observatories of the Carnegie Institution of Washington, 813 Santa Barbara Street, Pasadena, CA 91101, USA
[2] Department of Astrophysical Sciences, Princeton University, Princeton, NJ, USA
[3] Department of Astronomy, University of California, Berkeley, CA 94720-3411, USA
[4] Palomar Observatory, California Institute of Technology, MS 105-24, Pasadena, CA 91125, USA
Received 2008 September 11; accepted 2009 May 7; published 2009 June 16

ABSTRACT

We present new central stellar velocity dispersion measurements for 428 galaxies in the Palomar spectroscopic survey of bright, northern galaxies. Of these, 142 have no previously published measurements, most being relatively late-type systems with low velocity dispersions ($\lesssim$100 km s^{-1}). We provide updates to a number of literature dispersions with large uncertainties. Our measurements are based on a direct pixel-fitting technique that can accommodate composite stellar populations by calculating an optimal linear combination of input stellar templates. The original Palomar survey data were taken under conditions that are not ideally suited for deriving stellar velocity dispersions for galaxies with a wide range of Hubble types. We describe an effective strategy to circumvent this complication and demonstrate that we can still obtain reliable velocity dispersions for this sample of well-studied nearby galaxies.

Key words: galaxies: active – galaxies: kinematics and dynamics – galaxies: nuclei – galaxies: Seyfert – galaxies: starburst – surveys

Online-only material: machine-readable table

1. INTRODUCTION

The stellar velocity dispersion ($\sigma_\star$) of the central regions of galaxies is a parameter of considerable importance for a variety of extragalactic investigations. Since the early pioneering work of Burbidge et al. (1961) and Minkowski (1962), many techniques have been developed for measuring $\sigma_\star$ (e.g., Morton & Chevalier 1972; Richstone & Sargent 1972; Simkin 1974; Sargent et al. 1977; Tonry & Davis 1979; Bender 1990; Rix & White 1992; van der Marel & Franx 1993; Statler 1995; Barth et al. 2002; Cappellari & Emsellem 2004). Given the extensive body of observational material on $\sigma_\star$ for nearby galaxies, a number of catalogs have been compiled to consolidate the data. The most widely used of these are the catalog of Whitmore et al. (1985), which was updated by McElroy (1995), and of Prugniel et al. (1998), which is continuously updated and is available through the electronic database HyperLeda (Paturel et al. 2003).[6]

The vast majority of the published measurements of $\sigma_\star$ pertain to early-type galaxies, largely giant ellipticals and S0s. Significantly less data are available for galaxies along the spiral sequence, and those that have been published often show marked disagreement from study to study, as can be seen from perusal of the data tabulated in the above-mentioned catalogs. It is disconcerting that many of the highly discrepant entries are, in fact, associated with nearby, bright, well-studied galaxies. The scatter in the published values of $\sigma_\star$ can be blamed, at least in part, on the inherent heterogeneity of combining many disparate sources, which often employ different telescopes, detectors, apertures, observing strategies, and analysis techniques. The above-cited catalogs attempt to homogenize the final compilations by scaling the individual literature sources to a set of "standard" galaxies measured through a roughly constant aperture size ($2''\times4''$).

Notwithstanding these efforts, there is considerable motivation for assembling an independent, homogeneous, internally consistent set of new measurements, especially if the data cover a large sample of galaxies representing a wide range of Hubble types. A number of previous studies have been carried out with this goal in mind, mostly focused on relatively early-type galaxies (e.g., Davies et al. 1987; Bernardi et al. 2003). Our present paper adds to this effort using data taken as part of the Palomar spectroscopic survey of nearby galaxies. During the course of an extensive investigation primarily aimed at characterizing the nature of nuclear activity in nearby galaxies, we collected high-quality, moderate-resolution, long-slit optical spectra of the central regions of 486 bright, northern galaxies. The survey was conducted during the period 1984–1990; technical details of the survey and presentation of various data products and science results can be found in earlier papers in this series (Filippenko & Sargent 1985; Ho et al. 1995, 1997a, 1997b, 1997c, 1997d, 1997e, 2003). This contribution focuses on central stellar velocity dispersions extracted from the survey.

2. THE SURVEY

A full description of the Palomar survey is given by Ho et al. (1995, 1997a). Here we mention only a few pertinent details. The survey covers a nearly complete, magnitude-limited sample of 486 galaxies from the Revised Shapley–Ames Catalog (Sandage & Tammann 1981) that satisfies $B_T \leqslant 12.5$ mag and $\delta > 0^\circ$. The spectra were acquired using the Double Spectrograph (Oke & Gunn 1982) mounted at the Cassegrain focus of the Hale 5 m telescope at Palomar Observatory. A $2''$ wide slit was used for most of the survey. The spectra simultaneously cover the regions ~4230–5110 Å and ~6210–6860 Å. The average full width at half-maximum intensity (FWHM) spectral resolutions on the blue and red sides, as determined from comparison-lamp emission lines, are approximately 4.2 Å and 2.2 Å, respectively. These correspond to velocity resolutions, expressed as a Gaussian dispersion, of $\sigma_{\rm inst} = 118$ and 42 km

[5] Hubble Fellow, Princeton-Carnegie Fellow.
[6] http://leda.univ-lyon1.fr/

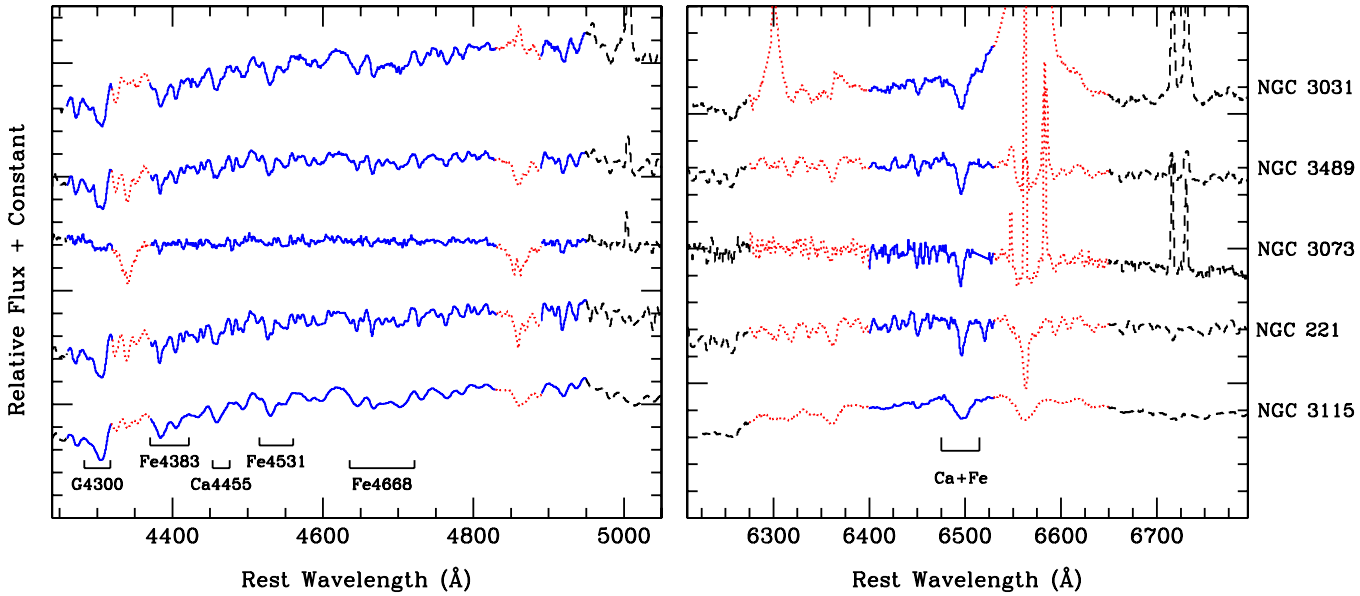

Figure 1. Sample blue (left) and red (right) spectra from the Palomar survey, adapted from Ho et al. (1995). The intensity of each spectrum has been scaled and arbitrarily shifted for clarity. The regions included in the fit are plotted in blue, while those masked from the fit are plotted as red dotted lines. Black dashed lines denote regions outside of the fitting window. The stellar metal-line indices defined by Ho et al. (1997a) are labeled on the bottom of each panel.

s^{-1} at 4500 Å and 6500 Å, respectively. (About 10% of the blue spectra were acquired in a slightly higher resolution mode with $\sigma_{\rm inst} = 74$ km s^{-1}.) The spectra analyzed in this paper are the same as those reported in the spectral atlas of Ho et al. (1995); they were extracted from a rectangular aperture of size $2'' \times 4''$, which is roughly equivalent to linear dimensions of 170 pc × 350 pc for a median distance of 17.9 Mpc (Ho et al. 1997a).

3. VELOCITY DISPERSIONS

3.1. Method

Our velocity dispersion measurements are based on the direct pixel-fitting method, which, as described by a number of authors (e.g., Rix & White 1992; van der Marel 1994; Kelson et al. 2000; Barth et al. 2002), has many of advantages compared to more traditional methods based on Fourier or cross-correlation techniques. The Palomar survey has several characteristics that pose special challenges for measuring accurate stellar velocity dispersions. First, the majority of the survey galaxies contain emission lines from active galactic nuclei (AGNs), often strong and of substantial velocity width, presenting a significant source of contamination for the stellar absorption features. Second, the spectral coverage of the survey was optimized for obtaining emission-line diagnostics and not for velocity dispersion measurements. Finally, the survey covers a very broad range of Hubble types, from dwarf irregulars to giant ellipticals. Galaxies with a wide range of stellar populations are especially susceptible to template mismatch. We use a modified version of the direct pixel-fitting code developed by Greene & Ho (2006). In brief, a nonlinear Levenberg–Marquardt minimization algorithm is used to compare the observed galaxy spectrum with a model spectrum $M(\lambda)$, which is assumed to be the convolution of a stellar template spectrum, $T(\lambda)$, and a line-of-sight velocity broadening function approximated as a Gaussian, $G(\lambda)$:

$$M(\lambda) = P(\lambda)\{[T(\lambda) \otimes G(\lambda)] + C(\lambda)\}. \quad (1)$$

Here, $C(\lambda)$ is an additive term to dilute the stellar features. It can be a power-law function to represent an AGN continuum, if present, or any other smooth component such as the featureless continuum from hot stars. For many of our later-type galaxies, adding a simple f_λ = constant term effectively mimics the continuum dilution of the metal lines by intermediate-age (A and early-F type) stars in the composite stellar population. The multiplicative factor $P(\lambda)$, typically chosen to be a third-order Legendre polynomial, accounts for large-scale mismatches in the continuum shapes of the galaxy and template star(s), which can arise from internal reddening in the galaxy, stellar population differences, and possible residual calibration errors.

An important improvement over the original code of Greene & Ho is that $T(\lambda)$, rather than being a single star, can be an optimal linear combination of several stars determined through a nonlinear least-squares fit. In the case of later-type spirals, especially, this modification provides a much better fit for their composite stellar populations, as well as a more robust determination of the final velocity dispersion of the galaxy because the intrinsic widths of the template stars vary with spectral type. Our approach of using a mixture of template stars is similar to those employed by several previous studies, including Rix & White (1992) and Cappellari & Emsellem (2004).

3.2. Fitting Regions

The blue setup just misses Mg I λ5175 ("Mg *b*"), the feature most commonly used to derive velocity dispersions in the visible part of the spectrum. Nevertheless, the blue spectra contain a significant number of relatively strong metal-line features, including the G band at 4300 Å, a calcium feature at 4455 Å, and iron features at 4383, 4531, and 4668 Å (Figure 1, left; see Table 7 in Ho et al. (1997a) for definitions of these stellar absorption-line indices). These metal-line features can be used to derive stellar velocity dispersions, so long as they are strong enough in the integrated spectrum. For the blue spectra we fit the region 4260–4950 Å; the blue end is chosen to include the G band, while the red end avoids the [O III] λλ4959, 5007 emission

lines. We mask the regions containing Hγ (4320–4370 Å) and Hβ (4830–4890 Å). In some strong emission-line objects, it is necessary to mask a small region around He II λ4686.

In practice, the above procedure works well for galaxies with a stellar population dominated by stars of spectral type mid-F and later, but not for those with younger populations. As Figure 1 illustrates, the spectrum of NGC 3073 contains mostly light from stars of type A and early-F, and the metal-line features, although clearly present in this spectrum of fairly high signal-to-noise ratio (S/N), are significantly diluted by the blue continuum of the hotter stars. Spectra like that of NGC 3073 (which, curiously, is an S0 galaxy) typically characterize many of the later-type spirals in the survey. The moderate resolution of the blue spectra presents another severe limitation. Even for galaxies where the blue metal-line features are strong and unambiguously detected (e.g., NGC 221 and NGC 3489 in Figure 1), the derived velocity dispersions may be subject to large systematic uncertainties if the true dispersions are near or below the native spectral resolution of $\sigma_{\rm inst} \approx 120$ km s^{-1}. For example, according to the literature NGC 221 and NGC 3489 have $\sigma = 72$ and 112 km s^{-1}, respectively.

The red spectra, with $\sigma_{\rm inst} \approx 40$ km s^{-1}, provide crucial relief to the many galaxies in the survey that suffer from insufficient resolution in the blue. Unfortunately, very few strong, uncontaminated stellar features exist in the spectral coverage of our red setup, which is dominated almost entirely by strong emission lines ([O I] $\lambda\lambda$6300, 6363, [N II] $\lambda\lambda$6548, 6583, Hα, and [S II] $\lambda\lambda$6716, 6731). One glimmer of hope lies with the Ca+Fe feature at 6495 Å. To the best of our knowledge, this little-known feature has never been used explicitly for kinematical measurements in galaxies, although it has played a role in other contexts such as the determination of radial-velocity curves for the secondary stars in black hole X-ray binaries (e.g., Filippenko et al. 1995, 1997). We will show that it plays a central role in our survey.

As Figure 1 (right) illustrates, the Ca+Fe feature, lying just blueward of the Hα+[N II] complex, is fairly well isolated, even in objects with prominent, broad Hα emission (e.g., NGC 3031). Importantly, it is moderately strong in nearly all galaxies, even those whose blue spectra are hopeless diluted by A and F-type stars (e.g., NGC 3073). Using the measurements published by Ho et al. (1997a, Table 9), we find that Ca+Fe was reliably detected in 438 out of the 486 galaxies in the Palomar survey (90%), with an average equivalent width of $\langle$W(Ca+Fe)$\rangle = 0.9$ Å. There is, at most, a factor of 2 variation in line strength from one extreme end of the Hubble sequence to the other. Among ellipticals and S0s (morphological type index $-6 < T < 0$; de Vaucouleurs et al. 1991), $\langle$W(Ca+Fe)$\rangle = 1.2$ Å, to be compared with $\langle$W(Ca+Fe)$\rangle = 0.6$ Å for Sc–Sdm spirals (morphological type index $5 < T < 9$).

After some experimentation, we find that the most stable fitting region for the red setup is 6400–6530 Å (Figure 1, right). The blue limit provides as much leverage as possible to define the continuum level without colliding with [O I] λ6363, and the red limit abuts [N II] λ6548. In a few objects with very strong, broad Hα emission, we had to curtail the red limit to 6510 Å; in these cases, it was often also helpful to increase the order of the polynomial factor (to ~5–6) to better trace the steeply rising gradient of the blue wing of the Hα emission line.

3.3. Template Stars

In addition to spectrophotometric standard stars, during the course of the survey we usually also took nightly observations of at least one late-type giant star to be used as a velocity template. Velocity standards were not observed in a small number of observing runs; this affected 50 galaxies, or roughly 10% of the survey. Because measuring velocity dispersions was not a top priority for the original survey, neither the number of stars nor their range of spectral types was chosen optimally. In some of the runs, only a single velocity template was observed, and at most there were two.

The limitations of the Palomar template stars compel us to explore an alternative calibration strategy. We use as our primary source of templates the library of Coudé-feed stellar spectra published by Valdes et al. (2004). This tremendously useful database contains high-S/N spectra of 1273 stars of essentially all spectral types, covering 3460 to 9464 Å. The spectral resolution of the library, FWHM ≈ 1 Å, is significantly higher than that of either the blue or red Palomar spectra. Thus, the Valdes stars can be used as velocity templates for the Palomar galaxies, after accounting for the differential instrumental broadening between the two data sets.

The Valdes library also gives us an extensive selection of stars of different spectral types for our optimal fit. Through experimentation, we find that in general a set of four stars—spectral types F6 III, G8 III, K0 III, and K3 III—suffices to account for the stellar population mixture of almost all galaxies in our sample. We give preference to stars of near-solar metallicity to try to approximate the conditions in galactic bulges. Although type-A and early-F stars clearly exist in some galaxies, in practice they do not need to be included because our fitting regions deliberately avoid the Balmer absorption lines (Figure 1) and the continuum dilution term ($C(\lambda)$ in Equation (1)) effectively mimics the hot continuum of these stars.

3.4. Fitting Results

Figure 2 gives examples of some typical fits. The top spectrum is that of the red giant (K0 III) star HD 107328, shown to help guide the eye to identify the stellar features. Subsequent spectra illustrate galaxies with a wide range in emission-line strengths and velocity dispersions. The original galaxy spectrum is plotted as black histograms; the best-fitting, optimally weighted, broadened velocity template is plotted as a thin blue line; and the masked regions are plotted as a red dotted line. Using a set of just four stars, we can usually achieve quite good fits, with formal statistical errors on the velocity dispersions in the range of 5%–10%. The results are also quite robust with respect to the choice of template stars; interchanging different stars of the same spectral type and similar metallicity affects the final dispersions at the level of 1% or less. In most objects, the largest fraction of the light comes, not surprisingly, from K giants. The Fe λ4668 feature, in particular, is very sensitive to K1 III–K3 III giant stars, which significantly improve the fit over the region 4600–4800 Å (Figure 3). Our fitting region for the red setup, especially the Ca+Fe λ6495 feature, is also very sensitive to K1 III–K3 III giants (Figure 4). The vast majority of the galaxies, however, including many bulge-dominated systems, require some contribution from G and even F-type stars.

To translate the Valdes-based dispersions onto the Palomar system, we subtract in quadrature the relative resolution difference between the Valdes and Palomar systems. Assuming the nominal instrumental resolutions of the two data sets, the resolution correction for the blue side is $\sigma_c = 114.8 \pm 5.8$ km s^{-1} (68.4 ± 7.1 km s^{-1} for the higher resolution mode), while that for the red side is $\sigma_c = 37.4 \pm 7.5$ km s^{-1}, where the

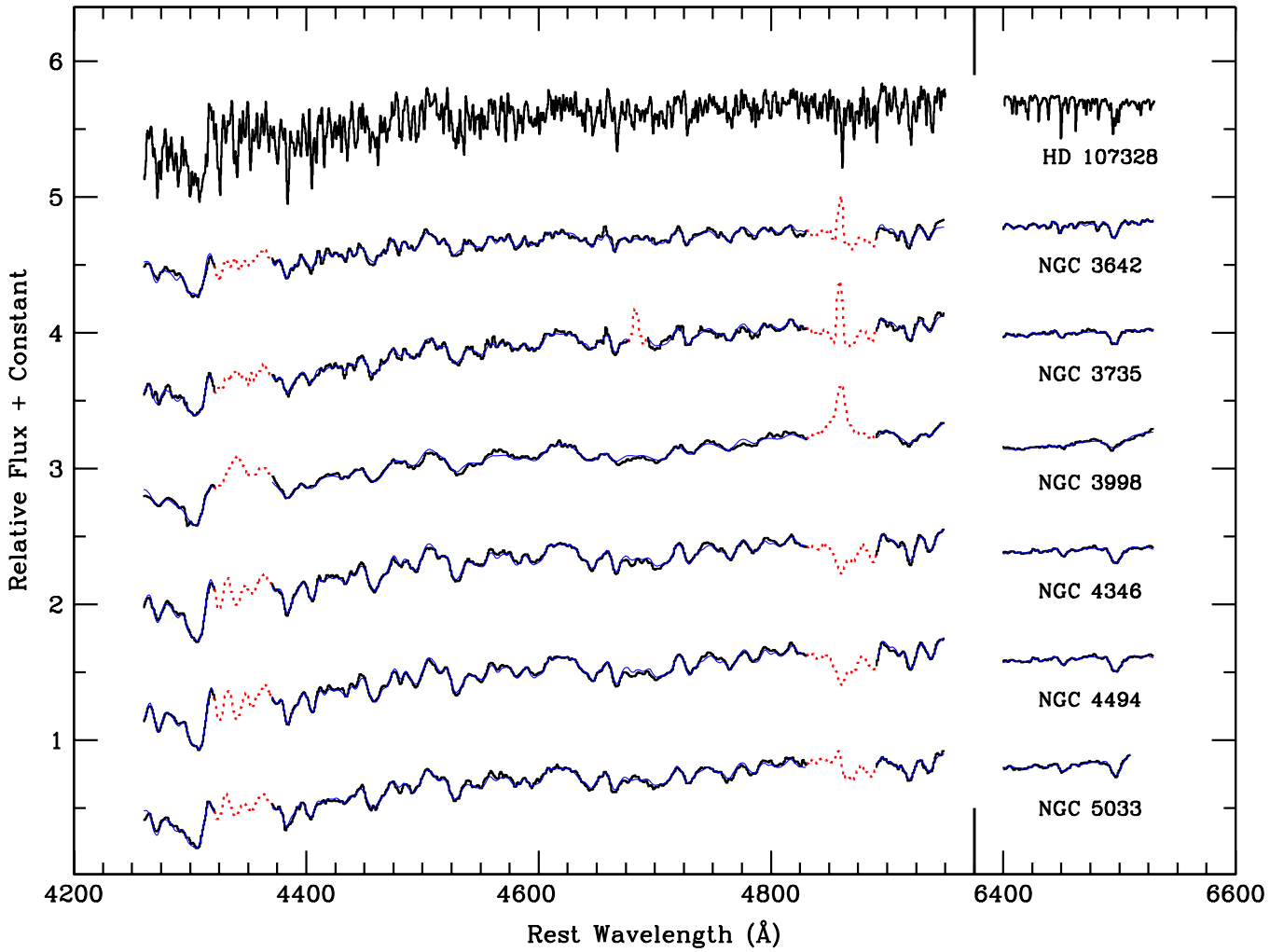

Figure 2. Sample fits for a representative set of galaxies. The top spectrum is that of the K0 III star HD 107328 from the Valdes et al. (2004) stellar library. For each galaxy, the original data are plotted as black histograms. The best-fitting model constructed from an optimal combination of broadened stellar templates is plotted as a thin blue curve. The regions excluded from the fit are marked as red dotted lines. The intensity of each spectrum has been scaled and arbitrarily shifted for clarity.

error bar represents the rms scatter of the night-to-night variations of the Palomar instrumental resolution. The validity of this simple approach can be verified empirically by comparing the corrected dispersions with published values. Among the 223 galaxies with velocity dispersions derived in the blue, 189 have literature measurements; of the 422 dispersions measured in the red, 283 have literature values. As illustrated in Figure 5, the adopted resolution corrections yield reasonably satisfactory agreement between our dispersion measurements and the literature values, particularly in the regime when the dispersions are well resolved ($\sigma \gtrsim \sigma_{\rm inst}$; solid points). On the blue side (Figure 5(a)), for $\sigma \gtrsim \sigma_{\rm inst} \approx 120$ km s^{-1}, $\langle \sigma_{\rm blue} - \sigma_{\rm Literature} \rangle = 1.2$ km s^{-1} with an rms scatter of 25.3 km s^{-1}. The red side delivers useful measurements down to $\sigma \approx \frac{1}{2}\sigma_{\rm inst} \approx 20$ km s^{-1} (Figure 5(b)). Over the entire velocity range, $\langle \sigma_{\rm red} - \sigma_{\rm Literature} \rangle = 3.0$ km s^{-1} with an rms scatter of 28.3 km s^{-1}. There is no perceptible systematic bias, provided that the optimal fit excludes the K3 III star, as explained below.

Our initial fits for the red-side spectra, which include the full complement of four template stars (F6 III to K3 III), revealed a puzzling systematic trend. Whereas the fits for low-σ galaxies yield dispersions that, after resolution correction, agree reasonably well with literature values, objects with $\sigma \gtrsim$ 150–200 km s^{-1} show a net systematic offset toward larger velocities, by roughly +30 km s^{-1}. We believe that this effect arises from template mismatch. As shown in Figure 4, in small, low-luminosity bulges, such as that in the Sc galaxy NGC 3631, the red absorption features, especially Ca+Fe, are nearly equally well fit by template stars of spectral type G8 III, K0 III, or K3 III. In stark contrast, NGC 3115, a luminous S0 galaxy with a substantial bulge, clearly singles out the K3 III star as the preferred template, which then contributes most of the weight to the optimal fit. (We have verified that K1 III and K2 III templates give almost equally good fits as the K3 III template.) Why? This is because the Ca+Fe feature is strongest in high-σ galaxies and in late-type giants. Within the Palomar galaxy sample, the strength of the Ca+Fe feature increases roughly with velocity dispersion, albeit with significant scatter. Dividing the sample into two, galaxies with $\sigma < 150$ km s^{-1} have $\langle$W(Ca+Fe)$\rangle = 0.87$ Å, to be compared with $\langle$W(Ca+Fe)$\rangle = 1.23$ Å for galaxies with $\sigma \geqslant 150$ km s^{-1}. At the same time, the strength of the Ca+Fe feature in stars increases toward later spectral types. To demonstrate this, we measured the Ca+Fe feature for individual stars in the Valdes library, using the index definition given in Ho et al. (1997a). Choosing 15 stars of roughly similar metallicities for each spectral type, we find $\langle$W(Ca+Fe)$\rangle = 0.79$, 0.99, 1.17, 1.35, and 1.53 Å for G8 III, K0 III, K1 III, K2 III, and K3 III, respectively. Galaxies with $\sigma \geqslant 150$ km s^{-1} have Ca+Fe strengths very similar to those of K1 III–K3 III stars, and

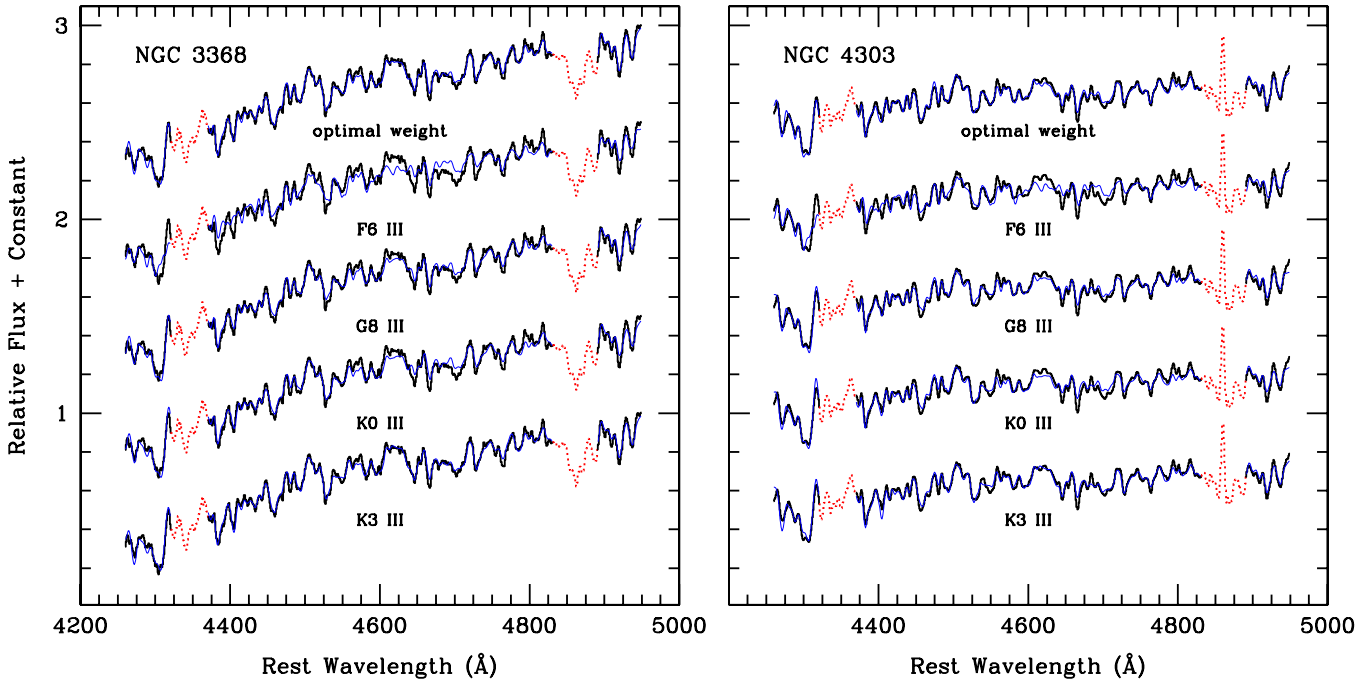

Figure 3. Sample fits for NGC 3368 and NGC 4303 in the blue spectral region. The top spectrum shows the optimally weighted fit, followed by fits using single stars of spectral type F6 III, G8 III, K0 III, and K3 III. The original data are plotted as black histograms, the fits are plotted as blue curves, and the regions excluded from the fit are plotted as red dotted lines. The intensity of each spectrum has been scaled and arbitrarily shifted for clarity.

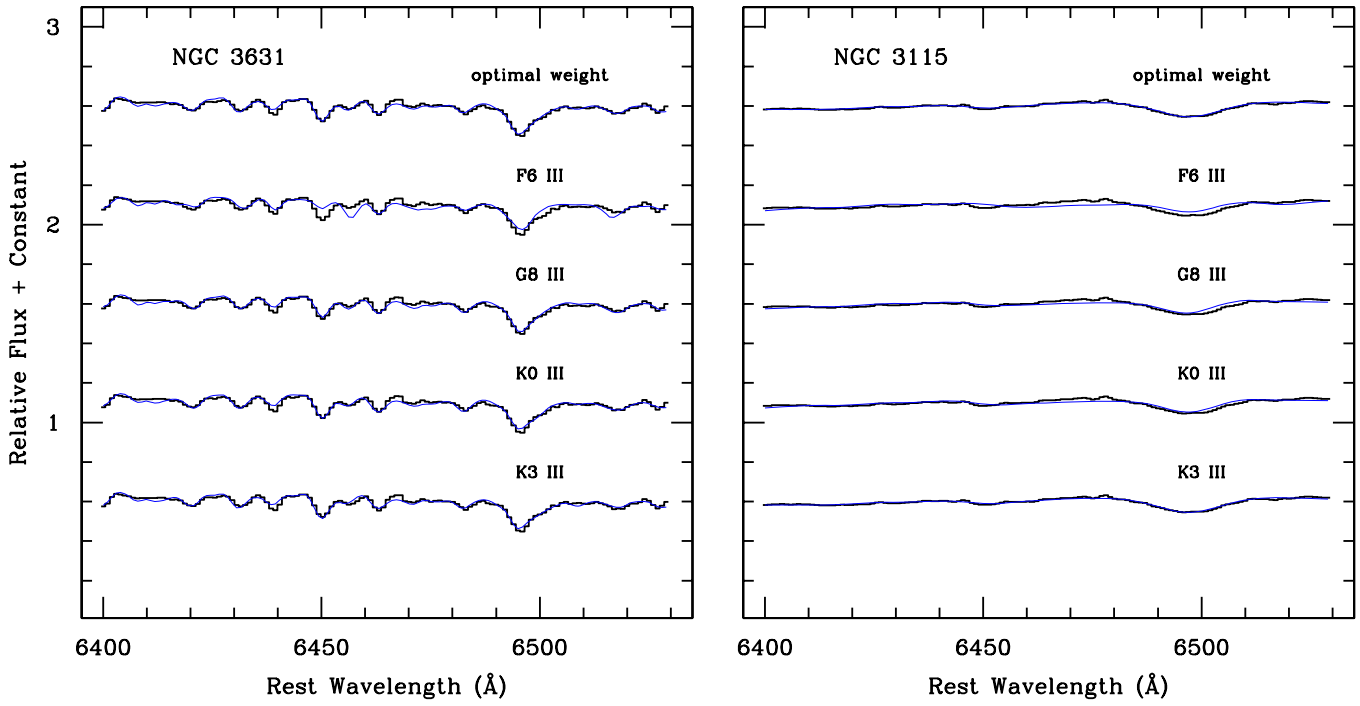

Figure 4. Sample fits for NGC 3631 and NGC 3115 in the red spectral region. The top spectrum shows the optimally weighted fit, followed by fits using single stars of spectral type F6 III, G8 III, K0 III, and K3 III. The original data are plotted as black histograms, and the fits are plotted as blue curves. The intensity of each spectrum has been scaled and arbitrarily shifted for clarity.

thus it is not surprising that an optimal fit would give these stars greatest weight. A bias in the derived velocity dispersion for high-σ galaxies arises *if* in these systems their Ca+Fe feature is boosted because of an abundance enhancement. We speculate that the culprit is Ca. As an α element, Ca may be enhanced similarly as Mg in early-type galaxies (Prochaska et al. 2005; but see Graves et al. 2007). In such a situation, the apparently good match with the K1 III–K3 III templates is only an artifact of their mutually strong Ca+Fe feature. Since such late-type giants have very narrow intrinsic line widths, the inferred velocity dispersion would be overestimated, thus leading to the observed bias. To bypass this complication, we removed the K3 III giant from the optimal fit of the red-side spectra.

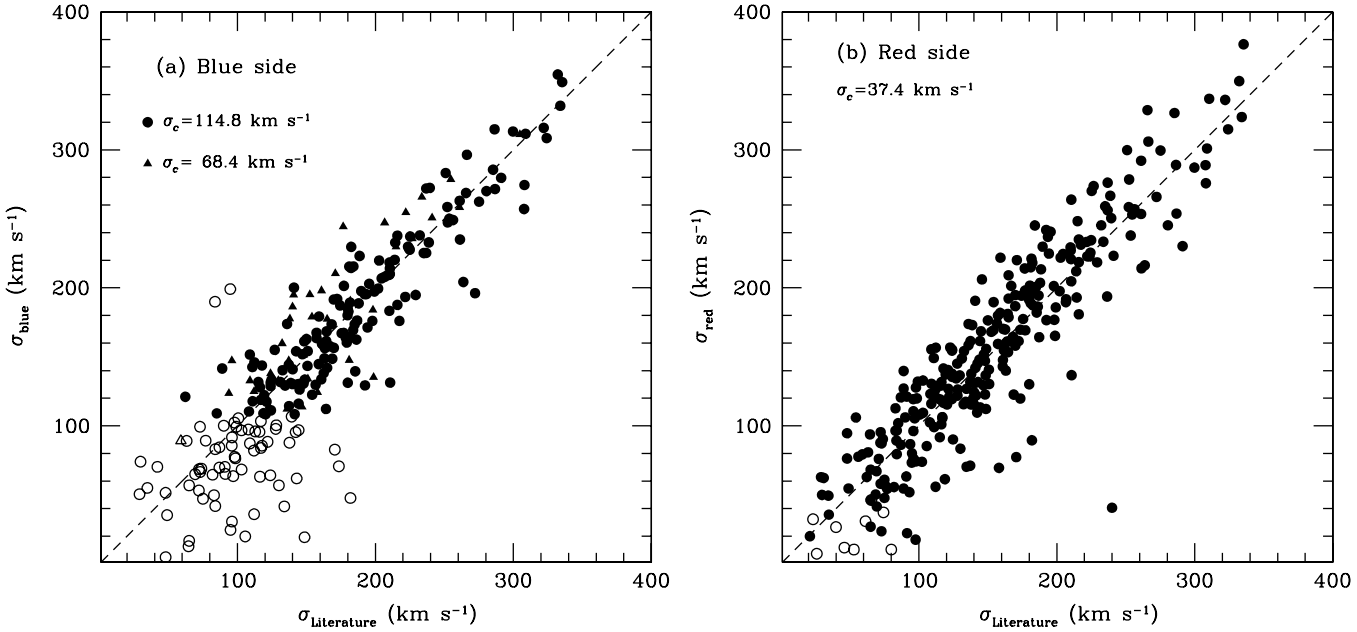

Figure 5. Comparison between velocity dispersions published in the literature with velocity dispersions derived using an optimal combination of Valdes template stars for the (a) blue side and (b) red side, corrected for the relative resolution difference (σ_c) between the Valdes and Palomar systems (see Section 3.3). Open symbols mark objects that are poorly resolved. The dashed diagonal line denotes equality.

For each galaxy, we compute a final velocity dispersion as the average of the blue-side and red-side dispersions, weighted by their respective error bars. The error bars reflect the quadrature sum of the formal statistical uncertainty from the optimal fit and the rms scatter of the resolution correction, which is dominated by the uncertainty in the original instrumental resolution of the Palomar spectra. Among the 428 galaxies with new velocity dispersion measurements, 286 have published literature values. Comparison between the objects in common (Figure 6) shows very good consistency. Over the entire range in velocities, $\langle\sigma_{\rm final} - \sigma_{\rm Literature}\rangle = 3.0$ km s^{-1}. The scatter is still quite large (rms 28.3 km s^{-1}), but its magnitude is consistent with that found by Barth et al. (2002) based on a smaller sample of ∼30 galaxies with high-quality velocity dispersion measurements.

There are several notable outliers in Figure 6, for which the literature values are larger than ours by more than ∼80 km s^{-1}. The most extreme case is NGC 520, for which HyperLeda reports $\sigma = 240 \pm 25$ km s^{-1} whereas we determine $\sigma = 40.6 \pm 8.9$ km s^{-1}. This is a complex, interacting galaxy (Arp 157), and the HyperLeda value of $\sigma = 240$ km s^{-1} pertains to the "southeast–northwest" component, not the primary nucleus of the "east–west" component (using the naming convention of Stanford & Balcells 1990a). The Palomar spectrum was centered on the position of the primary nucleus. From visual inspection of the plots published by Stanford & Balcells (1990a, 1990b), it appears that the published dispersion of the primary nucleus should be $\sigma \approx 100 \pm 25$ km s^{-1}. (We thank the referee for making this estimate for us, with which we agree.) The velocity dispersion for NGC 2967 (prior to homogenization), 200 ± 27 km s^{-1}, seems suspiciously high for an Sc galaxy; according to HyperLeda, it derives from an unpublished 1984 measurement by B. C. Whitmore and E. Malumuth. The same applies to the Sc galaxy NGC 4647, for which HyperLeda lists $\sigma = 98 \pm 39$ km s^{-1}. Finally, we note that the literature values of both NGC 3628 ($\sigma = 171 \pm 71$ km s^{-1}) and NGC 5364 ($\sigma = 91 \pm 52$ km s^{-1}) have exceptionally large error bars. If we exclude these five outliers from our sample, $\langle\sigma_{\rm final} - \sigma_{\rm Literature}\rangle = 2.7$ km s^{-1}, and the scatter reduces to 23.6 km s^{-1}.

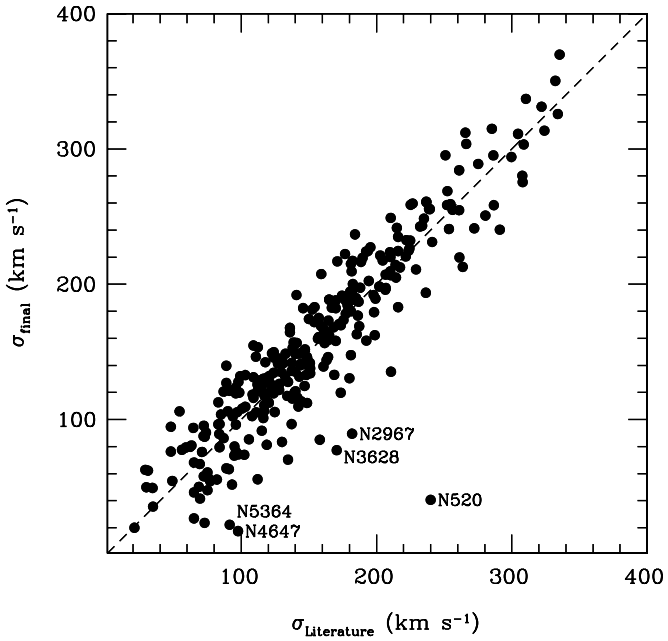

Figure 6. Comparison of final velocity dispersions with literature values. The dashed diagonal line denotes equality. Several prominent outliers are labeled (see Section 3.4).

4. THE CATALOG

The final results are presented in Table 1. For each galaxy, we list the literature value of the central stellar velocity dispersion, if available, followed by the dispersions derived from the blue ($\sigma_{\rm blue}$) and red ($\sigma_{\rm red}$) Palomar spectra, the final value ($\sigma_{\rm final}$) obtained from the weighted average of $\sigma_{\rm blue}$ and $\sigma_{\rm red}$, and lastly

Table 1
Catalog of Stellar Velocity Dispersions

Galaxy	Literature		Palomar				Adopted
	σ (km s^{-1})	Reference	$\sigma_{\rm blue}$ (km s^{-1})	$\sigma_{\rm red}$ (km s^{-1})	$\sigma_{\rm final}$ (km s^{-1})	Notes	σ (km s^{-1})
IC 10	...	...	...	...	...	1,2	35.5 ± 16.6
IC 239	...	...	92.3 ± 10.7	...	...	3,6,12	92.3 ± 10.7
IC 342	74.3 ± 11.4	1	...	...	...	2,7	74.3 ± 11.4
IC 356	141.0 ± 27.3	1	200.1 ± 15.9	142.0 ± 9.2	156.6 ± 8.0		156.6 ± 8.0
IC 467	...	...	...	64.2 ± 8.9	64.2 ± 8.9	8	64.2 ± 8.9
IC 520	...	...	126.6 ± 10.9	146.5 ± 9.3	138.1 ± 7.1		138.1 ± 7.1
IC 1727	...	...	...	136.8 ± 9.2	136.8 ± 9.2	6	136.8 ± 9.2
IC 2574	...	...	...	...	...	1,2	33.9 ± 15.9
NGC 63	...	...	...	25.6 ± 8.8	25.6 ± 8.8	2,7,12	25.6 ± 8.8
NGC 147	22.0 ± 5.0	1	...	...	...	2,9	22.0 ± 5.0
NGC 185	19.9 ± 2.4	1	...	...	...	2	19.9 ± 2.4
NGC 205	23.3 ± 3.7	1	...	...	...	2,7	23.3 ± 3.7
NGC 221	72.1 ± 1.9	1	...	87.7 ± 9.1	87.7 ± 9.1	6	72.1 ± 1.9
NGC 224	169.8 ± 5.2	1	191.5 ± 16.4	186.7 ± 9.9	188.0 ± 8.5		169.8 ± 5.2
NGC 266	...	...	209.3 ± 16.3	238.5 ± 10.8	229.6 ± 9.0		229.6 ± 9.0
NGC 278	...	...	...	47.6 ± 8.9	47.6 ± 8.9	6	47.6 ± 8.9
NGC 315	266.3 ± 22.8	1	296.4 ± 22.0	306.0 ± 12.2	303.7 ± 10.7		303.7 ± 10.7
NGC 404	40 ± 3	2	...	...	...	6,7	40 ± 3
NGC 410	299.7 ± 7.4	1	313.3 ± 19.5	287.1 ± 11.7	294.0 ± 10.0		299.7 ± 7.4
NGC 428	...	...	...	26.3 ± 8.5	26.3 ± 8.5	2,7,12	26.3 ± 8.5
NGC 474	163.4 ± 5.4	1	156.3 ± 12.7	160.4 ± 9.5	158.9 ± 7.6		163.4 ± 5.4
NGC 488	199.2 ± 9.8	1	197.3 ± 14.9	185.8 ± 9.9	189.3 ± 8.2		189.3 ± 8.2
NGC 507	307.7 ± 9.7	1	257.1 ± 19.3	288.9 ± 11.8	280.2 ± 10.1		307.7 ± 9.7
NGC 514	...	...	...	54.6 ± 8.6	54.6 ± 8.6	6	54.6 ± 8.6
NGC 520	240 ± 25	1	...	40.6 ± 8.9	40.6 ± 8.9	2,4,7,12	40.6 ± 8.9
NGC 521	...	...	214.9 ± 16.0	210.5 ± 10.3	211.8 ± 8.7		211.8 ± 8.7
NGC 524	253.5 ± 7.8	1	250.0 ± 19.1	237.9 ± 10.8	240.8 ± 9.4		253.5 ± 7.8
NGC 598	21 ± 3	3	...	20.0 ± 8.5	20.0 ± 8.5	2,7,11,12	21 ± 3
NGC 628	72.2 ± 7.8	1	...	58.0 ± 8.6	58.0 ± 8.6	6,8	72.2 ± 7.8
NGC 660	128 ± 6	2	...	121.9 ± 9.0	121.9 ± 9.0	3,6,8	128 ± 6
NGC 672	...	...	...	...	...	1,2	<64.3
NGC 676	...	...	135.0 ± 12.2	156.5 ± 10.3	147.6 ± 7.9		147.6 ± 7.9
NGC 697	...	...	...	75.0 ± 8.9	75.0 ± 8.9	6	75.0 ± 8.9
NGC 718	134 ± 20	1	...	117.4 ± 9.5	117.4 ± 9.5	6	117.4 ± 9.5
NGC 772	127.8 ± 5.2	1	...	145.1 ± 9.3	145.1 ± 9.3	6	127.8 ± 5.2
NGC 777	324.1 ± 10.6	1	308.5 ± 22.8	314.9 ± 12.3	313.5 ± 10.8		324.1 ± 10.6
NGC 783	...	...	...	101.4 ± 9.3	101.4 ± 9.3	6	101.4 ± 9.3
NGC 784	...	...	...	...	...	1,2	35.5 ± 16.6
NGC 812	...	...	...	120.9 ± 9.0	120.9 ± 9.0	6	120.9 ± 9.0
NGC 818	...	...	133.7 ± 12.3	164.2 ± 10.5	151.3 ± 8.0		151.3 ± 8.0
NGC 821	210.4 ± 3.6	1	210.1 ± 14.1	204.7 ± 10.3	206.6 ± 8.3		210.4 ± 3.6
NGC 841	...	...	177.0 ± 16.3	153.4 ± 9.3	159.2 ± 8.1		159.2 ± 8.1
NGC 864	65 ±	4	...	26.9 ± 9.0	26.9 ± 9.0	6,7,12	26.9 ± 9.0
NGC 877	...	...	...	105.8 ± 8.8	105.8 ± 8.8	6	105.8 ± 8.8
NGC 890	229.2 ± 9.9	1	194.8 ± 15.5	218.5 ± 10.6	210.9 ± 8.7		210.9 ± 8.7
NGC 891	73.1 ± 10.2	1	...	...	...	2	73.1 ± 10.2
NGC 925	...	...	...	...	...	1,2	<71.9
NGC 959	...	...	...	...	...	1,2,7	43.6 ± 20.4
NGC 972	...	...	...	102.8 ± 9.6	102.8 ± 9.6		102.8 ± 9.6
NGC 1003	...	...	...	...	...	2,5	...
NGC 1023	204.5 ± 4.2	1	206.9 ± 13.1	224.5 ± 10.5	217.6 ± 8.2		204.5 ± 4.2
NGC 1052	215 ± 4	2	229.7 ± 14.9	248.3 ± 11.2	241.6 ± 9.0		215 ± 4
NGC 1055	80 ± 15	1	...	...	...	3,5	80 ± 15
NGC 1058	31 ± 6	2	...	62.2 ± 8.4	62.2 ± 8.4	6	31 ± 6
NGC 1068	198.7 ± 17.0	1	135.2 ± 29.1	165.2 ± 9.6	162.3 ± 9.1		162.3 ± 9.1
NGC 1073	...	...	...	24.8 ± 8.7	24.8 ± 8.7	6,7,12	24.8 ± 8.7
NGC 1156	...	...	...	...	...	1,2	35.9 ± 16.8
NGC 1161	286.7 ± 16.4	1	271.6 ± 18.7	253.8 ± 11.1	258.4 ± 9.5		258.4 ± 9.5
NGC 1167	171 ±	5	210.4 ± 15.0	220.1 ± 10.5	216.9 ± 8.6		216.9 ± 8.6
NGC 1169	152.5 ± 25.4	1	195.1 ± 9.9	168.1 ± 9.7	181.3 ± 6.9		181.3 ± 6.9
NGC 1186	139.3 ± 29.5	1	...	119.8 ± 9.5	119.8 ± 9.5	6	119.8 ± 9.5
NGC 1275	258.9 ± 13.4	1	...	...	...	2	258.9 ± 13.4
NGC 1358	176.7 ± 10.1	1	244.3 ± 16.8	214.0 ± 10.3	222.3 ± 8.8		222.3 ± 8.8
NGC 1560	...	...	...	...	...	1,2	33.9 ± 15.9

Table 1
(Continued)

Galaxy	Literature		Palomar				Adopted
	σ (km s^{-1})	Reference	$\sigma_{\rm blue}$ (km s^{-1})	$\sigma_{\rm red}$ (km s^{-1})	$\sigma_{\rm final}$ (km s^{-1})	Notes	σ (km s^{-1})
NGC 1569	...	...	...	...	...	1,2	44.0 ± 20.6
NGC 1667	187.2 ± 27.0	1	176.1 ± 12.8	164.2 ± 10.3	168.9 ± 8.0		168.9 ± 8.0
NGC 1961	272.2 ± 46.6	1	196.1 ± 15.3	265.9 ± 11.3	241.3 ± 9.1		241.3 ± 9.1
NGC 2146	121.3 ± 33.9	1	...	126.8 ± 10.5	126.8 ± 10.5	2	126.8 ± 10.5
NGC 2268	...	...	112.3 ± 15.9	156.3 ± 10.3	143.3 ± 8.6		143.3 ± 8.6
NGC 2273	122.7 ± 9.9	1	114.3 ± 21.9	156.7 ± 10.4	148.9 ± 9.4		148.9 ± 9.4
NGC 2276	...	...	...	83.5 ± 9.5	83.5 ± 9.5	2	83.5 ± 9.5
NGC 2300	261.1 ± 6.1	1	263.0 ± 19.1	292.1 ± 11.7	284.2 ± 10.0		261.1 ± 6.1
NGC 2336	141.5 ± 12.1	1	108.4 ± 10.4	122.0 ± 9.0	116.2 ± 6.8		116.2 ± 6.8
NGC 2339	...	...	...	187.5 ± 10.1	187.5 ± 10.1	8	187.5 ± 10.1
NGC 2342	...	...	...	147.3 ± 10.6	147.3 ± 10.6	8	147.3 ± 10.6
NGC 2366	...	...	...	...	...	2	...
NGC 2403	...	...	...	...	...	1,6,7	68.4 ± 32.0
NGC 2500	...	...	...	...	...	1,2,7	47.1 ± 22.1
NGC 2537	...	...	...	63.0 ± 9.1	63.0 ± 9.1	2	63.0 ± 9.1
NGC 2541	53 ± 10	1	...	...	...	2	53 ± 10
NGC 2543	...	...	163.4 ± 20.8	101.3 ± 9.7	112.4 ± 8.8		112.4 ± 8.8
NGC 2549	142.6 ± 3.8	1	154.0 ± 11.5	145.2 ± 9.3	148.7 ± 7.2		142.6 ± 3.8
NGC 2634	181.1 ± 4.7	1	164.1 ± 13.4	188.8 ± 10.0	180.0 ± 8.0		181.1 ± 4.7
NGC 2639	198.2 ± 10.5	1	183.9 ± 13.0	176.8 ± 9.7	179.3 ± 7.8		179.3 ± 7.8
NGC 2655	162.5 ± 11.2	1	138.2 ± 14.3	169.8 ± 9.7	159.8 ± 8.0		159.8 ± 8.0
NGC 2681	109.1 ± 6.7	1	132.8 ± 13.4	130.5 ± 9.1	131.2 ± 7.5		109.1 ± 6.7
NGC 2683	116.4 ± 10.9	1	127.9 ± 11.2	131.7 ± 9.0	130.2 ± 7.0		130.2 ± 7.0
NGC 2685	93.8 ± 4.9	1	123.5 ± 10.0	86.7 ± 8.6	102.3 ± 6.5		93.8 ± 4.9
NGC 2715	...	...	...	84.6 ± 9.0	84.6 ± 9.0	6	84.6 ± 9.0
NGC 2742	65.6 ± 28.9	1	...	...	...	6,7	65.6 ± 28.9
NGC 2748	83 ± 8	6	...	96.4 ± 9.5	96.4 ± 9.5	6	83 ± 8
NGC 2750	...	...	...	52.4 ± 9.5	52.4 ± 9.5	8	52.4 ± 9.5
NGC 2768	181.8 ± 3.6	1	190.6 ± 12.7	196.0 ± 10.1	193.9 ± 7.9		181.8 ± 3.6
NGC 2770	...	...	...	81.0 ± 8.9	81.0 ± 8.9	6	81.0 ± 8.9
NGC 2775	175.5 ± 7.8	1	167.1 ± 12.3	177.4 ± 9.7	173.5 ± 7.6		173.5 ± 7.6
NGC 2776	75 ± 11.3	1	...	47.7 ± 8.6	47.7 ± 8.6	6	47.7 ± 8.6
NGC 2782	154.2 ± 23.3	1	122.5 ± 30.6	189.6 ± 10.0	183.1 ± 9.5		183.1 ± 9.5
NGC 2787	202 ± 5	2	199.5 ± 13.5	197.6 ± 10.1	198.3 ± 8.1		202 ± 5
NGC 2832	334.0 ± 7.4	1	331.9 ± 21.6	323.8 ± 12.5	325.8 ± 10.8		334.0 ± 7.4
NGC 2841	222 ± 4	2	254.6 ± 15.7	222.8 ± 10.5	232.6 ± 8.7		222 ± 4
NGC 2859	179.8 ± 10.9	1	180.1 ± 13.1	192.8 ± 9.9	188.2 ± 7.9		188.2 ± 7.9
NGC 2903	89 ± 4	6	...	139.7 ± 10.5	139.7 ± 10.5	2	89 ± 4
NGC 2911	233.7 ± 16.1	1	265.8 ± 16.1	233.4 ± 10.6	243.2 ± 8.9		243.2 ± 8.9
NGC 2950	185.4 ± 9.8	1	139.5 ± 11.0	182.1 ± 9.9	163.0 ± 7.4		163.0 ± 7.4
NGC 2964	103 ± 12	6	...	109.4 ± 9.8	109.4 ± 9.8	6	109.4 ± 9.8
NGC 2967	181.9 ± 24.6	1	...	89.5 ± 9.5	89.5 ± 9.5	6	89.5 ± 9.5
NGC 2976	...	...	...	...	...	1,6,7	36.0 ± 16.8
NGC 2977	...	...	...	104.5 ± 9.3	104.5 ± 9.3	6	104.5 ± 9.3
NGC 2985	140.8 ± 4.7	1	194.9 ± 14.6	190.6 ± 10.0	192.0 ± 8.3		140.8 ± 4.7
NGC 3003	...	...	...	...	...	1,2,7	44.1 ± 20.6
NGC 3027	...	...	...	25.6 ± 9.1	25.6 ± 9.1	1,6,7,12	25.6 ± 9.1
NGC 3031	161.6 ± 3.1	1	159.1 ± 11.0	154.6 ± 9.5	156.5 ± 7.2		161.6 ± 3.1
NGC 3034	129.5 ± 27.8	1	...	...	...	2	129.5 ± 27.8
NGC 3041	97 ± 30	1	...	105.4 ± 9.4	105.4 ± 9.4	6	105.4 ± 9.4
NGC 3043	...	...	...	51.9 ± 9.0	51.9 ± 9.0	2	51.9 ± 9.0
NGC 3073	34.8 ± 3.9	1	...	35.6 ± 8.7	35.6 ± 8.7	2,7,12	35.6 ± 8.7
NGC 3077	...	...	...	...	...	1,2,6,7	32.4 ± 15.2
NGC 3079	145.7 ± 9.7	1	130.5 ± 15.8	206.1 ± 10.7	182.3 ± 8.9		182.3 ± 8.9
NGC 3115	252.1 ± 5.9	1	258.6 ± 17.1	258.5 ± 11.1	258.5 ± 9.3		252.1 ± 5.9
NGC 3147	261.3 ± 22.2	1	235.0 ± 16.7	214.1 ± 10.2	219.8 ± 8.7		219.8 ± 8.7
NGC 3162	89 ± 2	6	141.5 ± 26.2	54.5 ± 9.1	63.9 ± 8.6		89 ± 2
NGC 3166	112.3 ± 23.1	1	146.0 ± 14.4	156.6 ± 9.5	153.4 ± 7.9		153.4 ± 7.9
NGC 3169	165.0 ± 16.4	1	177.4 ± 17.7	192.2 ± 10.0	188.6 ± 8.7		188.6 ± 8.7
NGC 3184	...	...	...	43.3 ± 8.9	43.3 ± 8.9	2,7,12	43.3 ± 8.9
NGC 3185	59.1 ± 19.4	1	...	79.3 ± 9.2	79.3 ± 9.2	6	79.3 ± 9.2
NGC 3190	169 ± 11	7	167.3 ± 14.6	198.0 ± 10.1	188.1 ± 8.3		188.1 ± 8.3
NGC 3193	194.3 ± 5.9	1	171.3 ± 12.5	224.8 ± 10.6	202.4 ± 8.1		194.3 ± 5.9
NGC 3198	65 ± 10	1	...	46.1 ± 8.7	46.1 ± 8.7	6,7,12	46.1 ± 8.7

Table 1
(Continued)

Galaxy	Literature		Palomar				Adopted
	σ (km s^{-1})	Reference	$\sigma_{\rm blue}$ (km s^{-1})	$\sigma_{\rm red}$ (km s^{-1})	$\sigma_{\rm final}$ (km s^{-1})	Notes	σ (km s^{-1})
NGC 3226	193.5 ± 5.1	1	195.4 ± 16.1	236.9 ± 10.6	224.4 ± 8.9		193.5 ± 5.1
NGC 3227	136 ± 4	8	...	...	...	2	136 ± 4
NGC 3245	209.9 ± 8.4	1	209.3 ± 17.1	229.3 ± 10.6	223.7 ± 9.0		209.9 ± 8.4
NGC 3254	117.8 ± 4.1	1	143.7 ± 11.8	141.5 ± 9.2	142.3 ± 7.3		117.8 ± 4.1
NGC 3294	75.9 ± 20.4	1	...	56.4 ± 8.7	56.4 ± 8.7	6	56.4 ± 8.7
NGC 3301	121.1 ± 9.8	1	117.5 ± 12.4	140.4 ± 9.2	132.3 ± 7.4		132.3 ± 7.4
NGC 3310	84 ± 1	6	...	96.6 ± 10.1	96.6 ± 10.1	6	84 ± 1
NGC 3319	...	...	...	87.4 ± 9.2	87.4 ± 9.2	8	87.4 ± 9.2
NGC 3338	86.9 ± 17.2	1	...	120.6 ± 9.6	120.6 ± 9.6	6	120.6 ± 9.6
NGC 3344	...	...	...	73.6 ± 9.1	73.6 ± 9.1	6	73.6 ± 9.1
NGC 3346	48 ±	4	...	76.3 ± 8.4	76.3 ± 8.4	8	76.3 ± 8.4
NGC 3348	236.4 ± 10.4	1	...	193.7 ± 12.4	193.7 ± 12.4	3,8	236.4 ± 10.4
NGC 3351	98.5 ± 20.3	1	...	119.9 ± 9.0	119.9 ± 9.0	6	119.9 ± 9.0
NGC 3359	...	...	...	55.3 ± 8.9	55.3 ± 8.9	8	55.3 ± 8.9
NGC 3367	...	...	...	61.2 ± 10.1	61.2 ± 10.1	2	61.2 ± 10.1
NGC 3368	128.2 ± 4.0	1	...	126.3 ± 9.0	126.3 ± 9.0	6	128.2 ± 4.0
NGC 3370	48.0 ± 27.9	1	...	94.6 ± 9.4	94.6 ± 9.4	6	94.6 ± 9.4
NGC 3377	138.7 ± 2.6	1	131.0 ± 12.3	173.0 ± 9.7	156.9 ± 7.6		138.7 ± 2.6
NGC 3379	206.7 ± 2.4	1	247.2 ± 16.0	191.7 ± 9.9	207.1 ± 8.4		206.7 ± 2.4
NGC 3384	148.4 ± 3.4	1	161.2 ± 11.5	136.7 ± 9.2	146.3 ± 7.2		148.4 ± 3.4
NGC 3389	...	...	69.3 ± 14.6	...	69.3 ± 14.6	3,6,9,12	69.3 ± 14.6
NGC 3395	...	...	96.5 ± 14.6	...	96.5 ± 14.6	3,6,9,12	96.5 ± 14.6
NGC 3412	100.7 ± 2.3	1	...	108.1 ± 8.8	108.1 ± 8.8	6	100.7 ± 2.3
NGC 3414	236.8 ± 7.5	1	272.0 ± 17.9	256.2 ± 11.1	260.6 ± 9.4		236.8 ± 7.5
NGC 3423	49 ±	4	...	54.6 ± 8.5	54.6 ± 8.5	6	54.6 ± 8.5
NGC 3430	...	...	...	50.4 ± 8.9	50.4 ± 8.9	6	50.4 ± 8.9
NGC 3432	...	...	...	...	...	1,2	37.0 ± 17.3
NGC 3433	...	...	...	80.0 ± 8.7	80.0 ± 8.7	6	80.0 ± 8.7
NGC 3448	...	...	...	...	...	1,2	50.7 ± 23.8
NGC 3486	65 ± 3	2	...	68.2 ± 8.4	68.2 ± 8.4	6	65 ± 3
NGC 3489	112 ± 3	2	...	120.9 ± 9.0	120.9 ± 9.0	6	112 ± 3
NGC 3495	...	...	...	60.4 ± 9.0	60.4 ± 9.0	6	60.4 ± 9.0
NGC 3504	123.9 ± 18.2	1	...	119.3 ± 10.3	119.3 ± 10.3	6	119.3 ± 10.3
NGC 3507	...	...	...	85.5 ± 9.0	85.5 ± 9.0	6	85.5 ± 9.0
NGC 3516	181 ± 5	8	147.6 ± 21.6	...	147.6 ± 21.6	2	181 ± 5
NGC 3521	180 ± 39	9	131.2 ± 11.4	130.1 ± 9.1	130.5 ± 7.1		130.5 ± 7.1
NGC 3556	...	...	...	79.4 ± 9.6	79.4 ± 9.6	2	79.4 ± 9.6
NGC 3583	142.9 ± 47.3	1	...	131.7 ± 10.1	131.7 ± 10.1	6	131.7 ± 10.1
NGC 3593	54.4 ± 7.2	1	...	106.0 ± 8.9	106.0 ± 8.9	6	54.4 ± 7.2
NGC 3596	...	...	...	103.0 ± 9.4	103.0 ± 9.4	6	103.0 ± 9.4
NGC 3600	...	...	...	49.8 ± 9.1	49.8 ± 9.1	8	49.8 ± 9.1
NGC 3607	224.9 ± 8.8	1	227.6 ± 15.4	234.5 ± 10.7	232.3 ± 8.8		232.3 ± 8.8
NGC 3608	192.2 ± 3.5	1	195.4 ± 13.7	241.9 ± 10.8	224.1 ± 8.5		192.2 ± 3.5
NGC 3610	161.2 ± 4.6	1	159.6 ± 13.1	170.2 ± 10.7	166.0 ± 8.3		161.2 ± 4.6
NGC 3613	210.3 ± 9.0	1	218.4 ± 16.2	220.8 ± 10.5	220.1 ± 8.8		220.1 ± 8.8
NGC 3623	138 ± 3	2	177.5 ± 11.6	137.7 ± 9.1	152.9 ± 7.2		138 ± 3
NGC 3626	164.2 ± 11.1	1	112.2 ± 14.4	161.2 ± 9.6	146.1 ± 8.0		146.1 ± 8.0
NGC 3627	124 ± 3	2	137.9 ± 15.4	154.5 ± 9.7	149.8 ± 8.2		124 ± 3
NGC 3628	170.6 ± 70.6	1	...	77.3 ± 8.9	77.3 ± 8.9	6	77.3 ± 8.9
NGC 3631	...	...	...	43.9 ± 8.6	43.9 ± 8.6	6,7,12	43.9 ± 8.6
NGC 3640	181.6 ± 4.5	1	189.3 ± 14.1	221.1 ± 10.7	209.5 ± 8.5		181.6 ± 4.5
NGC 3642	158.1 ± 32.7	1	124.2 ± 14.5	69.5 ± 9.1	85.0 ± 7.7		85.0 ± 7.7
NGC 3646	...	...	137.1 ± 11.5	164.3 ± 9.6	153.1 ± 7.4		153.1 ± 7.4
NGC 3652	...	...	...	56.4 ± 8.3	56.4 ± 8.3	8	56.4 ± 8.3
NGC 3655	...	...	...	91.1 ± 9.4	91.1 ± 9.4	6	91.1 ± 9.4
NGC 3665	184.1 ± 9.2	1	215.5 ± 17.3	245.2 ± 10.9	236.8 ± 9.2		236.8 ± 9.2
NGC 3666	...	...	...	60.6 ± 8.7	60.6 ± 8.7	6	60.6 ± 8.7
NGC 3675	108 ± 4	2	...	102.5 ± 8.7	102.5 ± 8.7	6	108 ± 4
NGC 3681	...	...	...	92.0 ± 8.9	92.0 ± 8.9	6	92.0 ± 8.9
NGC 3684	...	...	...	43.0 ± 8.9	43.0 ± 8.9	6,7,12	43.0 ± 8.9
NGC 3686	...	...	...	151.3 ± 9.7	151.3 ± 9.7	2	151.3 ± 9.7
NGC 3690	...	...	...	143.9 ± 11.3	143.9 ± 11.3	2	143.9 ± 11.3
NGC 3692	...	...	...	113.6 ± 9.5	113.6 ± 9.5	6	113.6 ± 9.5
NGC 3705	109 ± 9	1	...	116.0 ± 9.0	116.0 ± 9.0	6	116.0 ± 9.0

Table 1
(Continued)

Galaxy	Literature		Palomar				Adopted
	σ (km s^{-1})	Reference	$\sigma_{\rm blue}$ (km s^{-1})	$\sigma_{\rm red}$ (km s^{-1})	$\sigma_{\rm final}$ (km s^{-1})	Notes	σ (km s^{-1})
NGC 3718	169.9 ± 18.1	1	···	158.1 ± 9.6	158.1 ± 9.6	2	158.1 ± 9.6
NGC 3726	69.5 ± 24.8	1	···	41.5 ± 9.2	41.5 ± 9.2	6,7,12	41.5 ± 9.2
NGC 3729	···	···	···	76.2 ± 9.1	76.2 ± 9.1	6	76.2 ± 9.1
NGC 3735	···	···	124.4 ± 15.0	148.0 ± 10.1	140.6 ± 8.4		140.6 ± 8.4
NGC 3738	···	···	···	49.1 ± 9.1	49.1 ± 9.1	2	49.1 ± 9.1
NGC 3756	···	···	···	47.6 ± 8.5	47.6 ± 8.5	6	47.6 ± 8.5
NGC 3780	···	···	···	89.8 ± 9.4	89.8 ± 9.4	6	89.8 ± 9.4
NGC 3810	64.6 ± 8.7	1	···	93.8 ± 9.5	93.8 ± 9.5	6	64.6 ± 8.7
NGC 3813	···	···	···	72.1 ± 9.2	72.1 ± 9.2	6	72.1 ± 9.2
NGC 3838	144.3 ± 12.8	1	116.0 ± 10.7	161.4 ± 9.5	141.4 ± 7.1		141.4 ± 7.1
NGC 3877	···	···	···	86.1 ± 9.2	86.1 ± 9.2	6	86.1 ± 9.2
NGC 3884	···	···	193.0 ± 13.7	217.3 ± 10.5	208.3 ± 8.3		208.3 ± 8.3
NGC 3893	105.7 ± 23.8	1	···	85.3 ± 8.7	85.3 ± 8.7	6	85.3 ± 8.7
NGC 3898	206.5 ± 7.4	1	208.7 ± 14.1	189.6 ± 9.9	195.9 ± 8.1		206.5 ± 7.4
NGC 3900	···	···	127.3 ± 11.6	146.8 ± 9.3	139.2 ± 7.3		139.2 ± 7.3
NGC 3917	···	···	···	38.0 ± 8.5	38.0 ± 8.5	6,7,12	38.0 ± 8.5
NGC 3938	29.1 ± 4.9	1	···	62.8 ± 8.4	62.8 ± 8.4	6	29.1 ± 4.9
NGC 3941	168.7 ± 13.1	1	148.6 ± 11.0	122.6 ± 9.0	133.0 ± 7.0		133.0 ± 7.0
NGC 3945	174.4 ± 10.2	1	187.2 ± 12.4	194.3 ± 10.0	191.5 ± 7.8		191.5 ± 7.8
NGC 3949	82 ± 2	6	···	55.6 ± 8.7	55.6 ± 8.7	6	82 ± 2
NGC 3953	116 ± 3	6	···	129.2 ± 9.0	129.2 ± 9.0	6	116 ± 3
NGC 3963	···	···	···	40.9 ± 8.7	40.9 ± 8.7	6,7,12	40.9 ± 8.7
NGC 3976	···	···	221.4 ± 18.2	180.0 ± 9.9	189.5 ± 8.7		189.5 ± 8.7
NGC 3982	73 ± 4	2	···	87.3 ± 9.0	87.3 ± 9.0	6	73 ± 4
NGC 3992	140 ± 20	10	186.3 ± 11.4	124.2 ± 9.1	148.4 ± 7.1		148.4 ± 7.1
NGC 3998	304.6 ± 10	1	311.1 ± 22.1	···	311.1 ± 22.1	9	304.6 ± 10
NGC 4013	···	···	···	86.5 ± 8.6	86.5 ± 8.6	6	86.5 ± 8.6
NGC 4026	177.2 ± 4.5	1	201.4 ± 15.7	169.2 ± 9.7	178.1 ± 8.3		177.2 ± 4.5
NGC 4036	181.1 ± 8.3	1	215.4 ± 13.1	214.9 ± 10.6	215.1 ± 8.2		215.1 ± 8.2
NGC 4041	95 ± 5	11	···	80.1 ± 9.0	80.1 ± 9.0	6,10	95 ± 5
NGC 4051	89 ± 3	8	···	127.0 ± 10.1	127.0 ± 10.1	2	89 ± 3
NGC 4062	93.2 ± 7.7	1	···	51.9 ± 8.4	51.9 ± 8.4	6	93.2 ± 7.7
NGC 4064	···	···	···	78.2 ± 8.9	78.2 ± 8.9	2	78.2 ± 8.9
NGC 4088	77 ± 2	6	···	54.3 ± 8.9	54.3 ± 8.9	6	77 ± 2
NGC 4096	···	···	···	79.5 ± 8.7	79.5 ± 8.7	6	79.5 ± 8.7
NGC 4100	···	···	···	75.5 ± 9.4	75.5 ± 9.4	8	75.5 ± 9.4
NGC 4102	150 ±	4	162.9 ± 24.5	176.4 ± 10.4	174.3 ± 9.6		174.3 ± 9.6
NGC 4111	147.9 ± 4.0	1	130.6 ± 11.4	147.1 ± 9.3	140.5 ± 7.2		147.9 ± 4.0
NGC 4123	···	···	···	25.6 ± 10.1	25.6 ± 10.1	6,7,8,12	25.6 ± 10.1
NGC 4124	68.7 ± 13.5	1	···	50.2 ± 8.5	50.2 ± 8.5	6	50.2 ± 8.5
NGC 4125	226.7 ± 7.6	1	235.7 ± 15.4	273.7 ± 11.8	259.6 ± 9.4		226.7 ± 7.6
NGC 4136	···	···	···	38.4 ± 8.7	38.4 ± 8.7	6,7,8,12	38.4 ± 8.7
NGC 4138	140.1 ± 15.8	1	130.2 ± 11.5	115.3 ± 8.9	120.9 ± 7.0		120.9 ± 7.0
NGC 4143	214.4 ± 15.5	1	232.8 ± 14.7	193.0 ± 9.6	204.9 ± 8.0		204.9 ± 8.0
NGC 4144	···	···	···	···	···	1,2	<64.3
NGC 4145	···	···	···	···	···	2,3	···
NGC 4150	87 ± 3	2	···	86.2 ± 9.4	86.2 ± 9.4	6	87 ± 3
NGC 4151	97 ± 3	8	···	···	···	2	97 ± 3
NGC 4152	···	···	···	62.3 ± 9.0	62.3 ± 9.0	6	62.3 ± 9.0
NGC 4157	90.1 ± 4.4	1	···	106.1 ± 8.8	106.1 ± 8.8	6	90.1 ± 4.4
NGC 4162	···	···	···	76.1 ± 8.9	76.1 ± 8.9	6	76.1 ± 8.9
NGC 4168	183.9 ± 3.7	1	169.4 ± 13.3	199.6 ± 10.2	188.4 ± 8.1		183.9 ± 3.7
NGC 4169	215.9 ± 30.6	1	187.6 ± 14.4	180.8 ± 9.9	183.0 ± 8.2		183.0 ± 8.2
NGC 4178	···	···	···	25.7 ± 9.1	25.7 ± 9.1	2,7,12	25.7 ± 9.1
NGC 4179	157.3 ± 7.9	1	167.4 ± 12.3	179.9 ± 9.8	175.0 ± 7.7		175.0 ± 7.7
NGC 4183	···	···	···	···	···	1,2,7	34.4 ± 16.1
NGC 4192	132.4 ± 7.1	1	159.7 ± 11.6	115.6 ± 8.9	131.9 ± 7.1		131.9 ± 7.1
NGC 4203	167 ± 3	2	157.7 ± 11.6	201.4 ± 10.1	182.6 ± 7.6		167 ± 3
NGC 4212	75 ± 2	6	···	60.9 ± 9.1	60.9 ± 9.1	6	75 ± 2
NGC 4214	···	···	···	···	···	1,2	51.6 ± 24.2
NGC 4216	206.8 ± 9.6	1	208.0 ± 13.0	190.9 ± 9.9	197.2 ± 7.9		197.2 ± 7.9
NGC 4217	91.3 ± 4.4	1	···	121.1 ± 9.4	121.1 ± 9.4	6	91.3 ± 4.4
NGC 4220	124.7 ± 14.7	1	133.3 ± 11.7	90.1 ± 8.7	105.5 ± 7.0		105.5 ± 7.0
NGC 4235	151 ± 10	12	134.1 ± 12.1	···	134.1 ± 12.1	9	151 ± 10

Table 1
(Continued)

Galaxy	Literature		Palomar				Adopted
	σ (km s^{-1})	Reference	$\sigma_{\rm blue}$ (km s^{-1})	$\sigma_{\rm red}$ (km s^{-1})	$\sigma_{\rm final}$ (km s^{-1})	Notes	σ (km s^{-1})
NGC 4236	...	...	...	...	...	1,2	<62.8
NGC 4242	...	...	...	...	...	2	...
NGC 4244	...	...	...	36.8 ± 9.2	36.8 ± 9.2	6,7,12	36.8 ± 9.2
NGC 4245	...	...	...	82.7 ± 8.6	82.7 ± 8.6	6	82.7 ± 8.6
NGC 4251	119.4 ± 5.1	1	122.2 ± 11.1	137.2 ± 9.1	131.2 ± 7.0		119.4 ± 5.1
NGC 4254	130.1 ± 15.3	1	...	83.4 ± 9.2	83.4 ± 9.2	6	83.4 ± 9.2
NGC 4258	148 ± 4	6	151.3 ± 13.0	122.7 ± 9.7	132.9 ± 7.8		148 ± 4
NGC 4261	308.8 ± 5.8	1	311.6 ± 22.7	301.0 ± 12.0	303.3 ± 10.6		308.8 ± 5.8
NGC 4262	189.7 ± 14.3	1	197.6 ± 15.6	229.8 ± 10.7	219.5 ± 8.8		219.5 ± 8.8
NGC 4267	164.6 ± 6.1	1	168.4 ± 12.3	153.4 ± 9.4	158.9 ± 7.5		164.6 ± 6.1
NGC 4273	...	...	...	58.1 ± 9.5	58.1 ± 9.5	2	58.1 ± 9.5
NGC 4274	137.2 ± 11.9	1	147.3 ± 12.0	71.1 ± 8.5	96.6 ± 6.9		96.6 ± 6.9
NGC 4278	261 ± 8	2	258.4 ± 19.5	253.5 ± 11.0	254.7 ± 9.6		261 ± 8
NGC 4281	280.5 ± 14.2	1	270.1 ± 20.9	245.3 ± 11.0	250.7 ± 9.7		250.7 ± 9.7
NGC 4291	285.3 ± 5.7	1	285.6 ± 20.7	326.7 ± 13.1	314.9 ± 11.1		285.3 ± 5.7
NGC 4293	148.6 ± 25.9	1	...	112.2 ± 9.2	112.2 ± 9.2	6	112.2 ± 9.2
NGC 4298	...	...	...	42.2 ± 8.7	42.2 ± 8.7	6,7,12	42.2 ± 8.7
NGC 4303	84 ± 3	6	...	79.5 ± 8.5	79.5 ± 8.5	6	84 ± 3
NGC 4314	117 ± 4	2	118.8 ± 10.9	105.5 ± 8.5	110.5 ± 6.7		117 ± 4
NGC 4321	83 ± 3	6	...	112.7 ± 8.9	112.7 ± 8.9	6	83 ± 3
NGC 4324	98.0 ± 3.5	1	...	74.2 ± 8.9	74.2 ± 8.9	6	98.0 ± 3.5
NGC 4339	112.9 ± 3.7	1	...	128.7 ± 9.1	128.7 ± 9.1	6	112.9 ± 3.7
NGC 4340	116.3 ± 2.9	1	...	101.1 ± 8.5	101.1 ± 8.5	6	116.3 ± 2.9
NGC 4346	...	...	150.5 ± 11.1	143.8 ± 9.2	146.5 ± 7.1		146.5 ± 7.1
NGC 4350	180.5 ± 7.2	1	182.8 ± 13.1	201.6 ± 10.2	194.5 ± 8.0		180.5 ± 7.2
NGC 4365	256.2 ± 3.3	1	249.1 ± 18.5	257.0 ± 11.1	254.9 ± 9.5		256.2 ± 3.3
NGC 4369	...	...	...	71.6 ± 9.1	71.6 ± 9.1	6	71.6 ± 9.1
NGC 4371	134.6 ± 4.5	1	129.2 ± 10.6	126.8 ± 9.1	127.8 ± 6.9		134.6 ± 4.5
NGC 4374	308 ± 7	2	274.5 ± 20.7	275.8 ± 11.5	275.5 ± 10.1		308 ± 7
NGC 4378	197.8 ± 9.6	1	176.0 ± 13.2	201.3 ± 10.1	192.0 ± 8.0		192.0 ± 8.0
NGC 4379	108.4 ± 4.1	1	110.4 ± 11.8	123.1 ± 9.1	118.4 ± 7.2		108.4 ± 4.1
NGC 4380	62.2 ± 18.2	1	121.0 ± 13.1	62.9 ± 8.4	79.8 ± 7.1		79.8 ± 7.1
NGC 4382	178.6 ± 4.8	1	163.9 ± 13.9	195.5 ± 10.1	184.6 ± 8.2		178.6 ± 4.8
NGC 4388	115.2 ± 17.1	1	...	91.7 ± 9.5	91.7 ± 9.5	2	91.7 ± 9.5
NGC 4394	137.7 ± 15.6	1	...	115.5 ± 8.9	115.5 ± 8.9		115.5 ± 8.9
NGC 4395	30 ±	13	...	...	...	2	30 ±
NGC 4405	...	...	...	...	...	1,6,7	50.2 ± 23.5
NGC 4406	235.0 ± 3.0	1	225.2 ± 16.7	259.1 ± 11.3	248.5 ± 9.4		235.0 ± 3.0
NGC 4414	117 ± 4	2	...	118.1 ± 9.0	118.1 ± 9.0	6	117 ± 4
NGC 4417	131.2 ± 6.2	1	131.7 ± 11.1	148.8 ± 9.4	141.7 ± 7.2		131.2 ± 6.2
NGC 4419	99.2 ± 3.2	1	...	132.0 ± 9.4	132.0 ± 9.4	6	99.2 ± 3.2
NGC 4421	112.1 ± 17.8	1	...	55.8 ± 8.3	55.8 ± 8.3	6	55.8 ± 8.3
NGC 4424	...	...	...	56.8 ± 9.2	56.8 ± 9.2	2	56.8 ± 9.2
NGC 4429	192.5 ± 7.5	1	129.3 ± 12.2	176.6 ± 9.7	158.3 ± 7.6		192.5 ± 7.5
NGC 4435	156.7 ± 5.8	1	129.7 ± 14.0	174.2 ± 9.7	159.8 ± 8.0		156.7 ± 5.8
NGC 4438	...	...	131.2 ± 10.8	139.0 ± 9.2	135.7 ± 7.0		135.7 ± 7.0
NGC 4442	186.7 ± 8.7	1	176.3 ± 12.3	194.4 ± 10.1	187.1 ± 7.8		187.1 ± 7.8
NGC 4448	173.5 ± 26.5	1	...	119.8 ± 9.0	119.8 ± 9.0	6	119.8 ± 9.0
NGC 4449	...	...	...	17.8 ± 9.1	17.8 ± 9.1	2,7,12	17.8 ± 9.1
NGC 4450	129.6 ± 15.5	1	133.0 ± 10.6	136.5 ± 9.1	135.0 ± 6.9		135.0 ± 6.9
NGC 4457	95.9 ± 15.1	1	...	119.3 ± 9.0	119.3 ± 9.0	6	119.3 ± 9.0
NGC 4459	169.9 ± 7.1	1	156.5 ± 14.1	194.7 ± 9.8	182.3 ± 8.0		169.9 ± 7.1
NGC 4460	...	...	...	39.8 ± 8.9	39.8 ± 8.9	2,7,12	39.8 ± 8.9
NGC 4461	150.8 ± 6.4	1	143.4 ± 11.3	140.7 ± 9.6	141.8 ± 7.3		150.8 ± 6.4
NGC 4469	...	...	109.6 ± 11.5	104.8 ± 9.3	106.7 ± 7.2		106.7 ± 7.2
NGC 4470	...	...	...	89.9 ± 9.0	89.9 ± 9.0	6	89.9 ± 9.0
NGC 4472	291.1 ± 2.9	1	279.7 ± 21.0	230.2 ± 10.6	240.3 ± 9.5		291.1 ± 2.9
NGC 4473	179.3 ± 2.9	1	160.3 ± 12.3	196.2 ± 10.1	181.7 ± 7.8		179.3 ± 2.9
NGC 4477	186.2 ± 15.2	1	162.5 ± 12.0	186.4 ± 9.8	176.8 ± 7.6		176.8 ± 7.6
NGC 4478	137.4 ± 2.3	1	114.3 ± 11.3	161.4 ± 9.5	141.9 ± 7.3		137.4 ± 2.3
NGC 4485	...	...	...	...	...	1,2,7	52.2 ± 24.4
NGC 4486	332.2 ± 4.9	1	354.6 ± 38.0	349.8 ± 13.0	350.3 ± 12.3		332.2 ± 4.9
NGC 4490	...	...	...	45.1 ± 9.0	45.1 ± 9.0	2,7,12	45.1 ± 9.0
NGC 4494	145 ± 3	2	126.3 ± 10.5	168.5 ± 9.5	149.5 ± 7.0		145 ± 3

Table 1
(Continued)

Galaxy	Literature		Palomar				Adopted
	σ (km s^{-1})	Reference	$\sigma_{\rm blue}$ (km s^{-1})	$\sigma_{\rm red}$ (km s^{-1})	$\sigma_{\rm final}$ (km s^{-1})	Notes	σ (km s^{-1})
NGC 4496A	...	...	...	...	...	1,2	74.9 ± 35.1
NGC 4496B	...	...	132.9 ± 22.6	100.6 ± 9.7	105.6 ± 8.9		105.6 ± 8.9
NGC 4501	160.9 ± 12.8	1	198.0 ± 11.9	147.7 ± 9.3	166.8 ± 7.3		166.9 ± 7.3
NGC 4503	110.8 ± 25.4	1	142.6 ± 11.3	149.1 ± 9.4	146.4 ± 7.2		146.4 ± 7.2
NGC 4517	...	...	...	43.8 ± 8.5	43.8 ± 8.5	7,8,12	43.8 ± 8.5
NGC 4526	263.7 ± 18.9	1	204.2 ± 16.2	216.3 ± 10.3	212.8 ± 8.7		212.8 ± 8.7
NGC 4527	210.7 ± 10.2	1	131.3 ± 15.7	136.7 ± 9.2	135.3 ± 7.9		135.3 ± 7.9
NGC 4532	...	...	...	...	...	1,2	<70.9
NGC 4535	...	...	...	102.5 ± 10.2	102.5 ± 10.2	8	102.5 ± 10.2
NGC 4536	85 ± 1	6	109.0 ± 16.5	101.9 ± 9.5	103.7 ± 8.2		85 ± 1
NGC 4548	144.3 ± 15	1	...	113.4 ± 8.9	113.4 ± 8.9	6	113.4 ± 8.9
NGC 4550	90.9 ± 4.4	1	...	63.3 ± 8.9	63.3 ± 8.9	6	90.9 ± 4.4
NGC 4552	252.4 ± 3.4	1	247.4 ± 17.2	278.5 ± 11.6	268.8 ± 9.6		252.4 ± 3.4
NGC 4559	...	...	...	49.2 ± 8.6	49.2 ± 8.6	6	49.2 ± 8.6
NGC 4564	157.4 ± 3.1	1	163.5 ± 11.8	159.3 ± 9.5	161.0 ± 7.4		157.4 ± 3.1
NGC 4565	136.0 ± 6.3	1	173.8 ± 11.6	158.4 ± 9.4	164.5 ± 7.3		136.0 ± 6.3
NGC 4567	...	...	...	66.0 ± 9.1	66.0 ± 9.1	6	66.0 ± 9.1
NGC 4568	...	...	...	88.3 ± 9.4	88.3 ± 9.4	6	88.3 ± 9.4
NGC 4569	136 ± 3	2	112.1 ± 29.2	173.8 ± 9.7	167.7 ± 9.2		136 ± 3
NGC 4570	187.9 ± 8.5	1	188.7 ± 12.1	203.6 ± 10.2	197.4 ± 7.8		197.4 ± 7.8
NGC 4578	120.4 ± 9.6	1	108.4 ± 10.1	115.5 ± 9.0	112.4 ± 6.7		112.4 ± 6.7
NGC 4579	165 ± 4	2	161.9 ± 12.3	209.1 ± 10.8	188.6 ± 8.1		165 ± 4
NGC 4589	224.3 ± 5.6	1	228.6 ± 16.4	225.5 ± 10.5	226.4 ± 8.8		224.3 ± 5.6
NGC 4594	241.1 ± 4.4	1	250.8 ± 16.4	223.2 ± 10.5	231.2 ± 8.8		241.1 ± 4.4
NGC 4596	148.8 ± 2.9	1	133.5 ± 11.0	155.7 ± 10.1	145.5 ± 7.4		148.8 ± 2.9
NGC 4605	...	...	...	26.1 ± 9.3	26.1 ± 9.3	6,7,12	26.1 ± 9.3
NGC 4608	160.8 ± 14.2	1	133.7 ± 11.2	143.0 ± 9.3	139.2 ± 7.2		139.2 ± 7.2
NGC 4612	63.2 ± 4.2	1	...	80.8 ± 8.5	80.8 ± 8.5	6	63.2 ± 4.2
NGC 4618	...	...	...	...	...	1,2	<54.6
NGC 4621	225.2 ± 3.3	1	237.2 ± 15.5	270.2 ± 11.3	258.7 ± 9.1		225.2 ± 3.3
NGC 4631	...	...	...	...	...	1,2	<71.9
NGC 4636	202.7 ± 3.4	1	219.8 ± 15.2	221.9 ± 10.5	221.2 ± 8.6		202.7 ± 3.4
NGC 4638	121.9 ± 4.0	1	...	120.9 ± 9.0	120.9 ± 9.0	6	121.9 ± 4.0
NGC 4639	96 ± 4	2	...	96.2 ± 9.1	96.2 ± 9.1	6	96 ± 4
NGC 4643	163 ± 7.9	1	148.8 ± 11.6	140.0 ± 10.0	143.8 ± 7.6		143.8 ± 7.6
NGC 4647	97.6 ± 38.8	1	...	17.5 ± 8.8	17.5 ± 8.8	6,7,12	17.5 ± 8.8
NGC 4648	215.9 ± 10.1	1	237.8 ± 15.8	218.6 ± 10.5	224.5 ± 8.7		224.5 ± 8.7
NGC 4649	335.3 ± 4.5	1	349.1 ± 23.6	376.5 ± 13.5	369.7 ± 11.7		335.3 ± 4.5
NGC 4651	...	...	...	100.9 ± 8.7	100.9 ± 8.7	6	100.9 ± 8.7
NGC 4654	...	...	...	47.7 ± 9.0	47.7 ± 9.0	8	47.7 ± 9.0
NGC 4656	...	...	...	...	...	1,8,9	70.4 ± 32.9
NGC 4660	188.5 ± 3.4	1	223.1 ± 15.2	213.4 ± 10.3	216.5 ± 8.5		188.5 ± 3.4
NGC 4665	...	...	168.0 ± 12.0	129.7 ± 9.1	143.7 ± 7.3		143.7 ± 7.3
NGC 4688	...	...	...	73.0 ± 8.8	73.0 ± 8.8	6	73.0 ± 8.8
NGC 4689	...	...	...	41.4 ± 8.4	41.4 ± 8.4	7,8,12	41.4 ± 8.4
NGC 4694	61.3 ± 6.5	1	...	...	...	2,7	61.3 ± 6.5
NGC 4698	132.7 ± 8.6	1	140.3 ± 11.6	154.1 ± 9.5	148.6 ± 7.3		148.6 ± 7.3
NGC 4710	142.2 ± 9.5	1	...	109.6 ± 9.5	109.6 ± 9.5	6	109.6 ± 9.5
NGC 4713	...	...	...	23.2 ± 8.9	23.2 ± 8.9	6,7,12	23.2 ± 8.9
NGC 4725	140 ± 3	2	141.0 ± 10.3	130.8 ± 9.1	135.3 ± 6.8		140 ± 3
NGC 4736	112 ± 3	2	125.0 ± 11.9	126.3 ± 9.8	125.8 ± 7.6		112 ± 3
NGC 4750	...	...	131.4 ± 11.0	139.2 ± 9.2	136.0 ± 7.1		136.0 ± 7.1
NGC 4754	184.9 ± 4.3	1	173.5 ± 12.3	200.7 ± 10.1	189.7 ± 7.8		184.9 ± 4.3
NGC 4762	147.1 ± 9.4	1	151.9 ± 11.3	151.7 ± 9.4	151.8 ± 7.2		151.8 ± 7.2
NGC 4772	...	...	152.3 ± 13.2	146.3 ± 9.4	148.3 ± 7.7		148.3 ± 7.7
NGC 4793	...	...	...	26.6 ± 8.5	26.6 ± 8.5	2,7,12	26.6 ± 8.5
NGC 4800	111 ± 4	2	117.8 ± 12.4	99.1 ± 8.7	105.3 ± 7.1		111 ± 4
NGC 4826	96 ± 3	2	147.3 ± 11.9	110.5 ± 8.9	123.7 ± 7.1		96 ± 3
NGC 4845	...	...	...	133.9 ± 9.3	133.9 ± 9.3	6	133.9 ± 9.3
NGC 4866	210.1 ± 9.7	1	183.3 ± 12.8	227.1 ± 10.5	209.5 ± 8.1		209.5 ± 8.1
NGC 4900	...	...	...	58.6 ± 9.0	58.6 ± 9.0	6	58.6 ± 9.0
NGC 4914	223.6 ± 25.1	1	229.8 ± 16.9	222.7 ± 10.5	224.7 ± 8.9		224.7 ± 8.9
NGC 5005	154 ± 10	6	178.9 ± 14.9	169.2 ± 9.6	172.0 ± 8.1		172.0 ± 8.1
NGC 5012	...	...	...	141.4 ± 9.2	141.4 ± 9.2	6	141.4 ± 9.2

Table 1
(Continued)

Galaxy	Literature		Palomar				Adopted
	σ (km s^{-1})	Reference	$\sigma_{\rm blue}$ (km s^{-1})	$\sigma_{\rm red}$ (km s^{-1})	$\sigma_{\rm final}$ (km s^{-1})	Notes	σ (km s^{-1})
NGC 5033	151 ± 4	2	154.1 ± 13.9	130.3 ± 9.4	137.8 ± 7.8		151 ± 4
NGC 5055	117 ± 6	6	...	106.3 ± 8.9	106.3 ± 8.9	6	117 ± 6
NGC 5077	254.6 ± 7.9	1	278.7 ± 19.7	253.1 ± 11.0	259.2 ± 9.6		254.6 ± 7.9
NGC 5112	...	...	...	...	...	1,6,7	<60.8
NGC 5147	...	...	...	52.3 ± 8.8	52.3 ± 8.8	6	52.3 ± 8.8
NGC 5194	96.0 ± 8.7	1	...	76.3 ± 9.1	76.3 ± 9.1	6	96.0 ± 8.7
NGC 5195	146.8 ± 15.1	1	113.8 ± 14.9	129.4 ± 9.7	124.8 ± 8.1		124.8 ± 8.1
NGC 5204	...	...	...	...	...	1,2	39.9 ± 18.7
NGC 5248	...	...	...	99.4 ± 9.2	99.4 ± 9.2	6	99.4 ± 9.2
NGC 5273	71 ± 4	2	...	76.0 ± 8.8	76.0 ± 8.8	6,8	71 ± 4
NGC 5297	118.9 ± 20.3	1	109.1 ± 10.6	61.3 ± 9.0	81.3 ± 6.9		61.3 ± 9.0
NGC 5300	...	...	...	19.8 ± 8.4	19.8 ± 8.4	2,7,12	19.8 ± 8.4
NGC 5308	210.5 ± 12.1	1	214.1 ± 17.3	263.9 ± 11.3	249.0 ± 9.5		249.0 ± 9.5
NGC 5322	232.2 ± 4.4	1	238.0 ± 17.0	245.3 ± 13.1	242.6 ± 10.4		232.2 ± 4.4
NGC 5353	286.4 ± 5.4	1	314.9 ± 20.7	289.0 ± 11.6	295.2 ± 10.1		286.4 ± 5.4
NGC 5354	217.4 ± 6.4	1	176.0 ± 14.6	231.3 ± 10.5	212.4 ± 8.5		217.4 ± 6.4
NGC 5363	195.5 ± 14.7	1	202.9 ± 14.8	240.6 ± 10.9	227.3 ± 8.8		227.3 ± 8.8
NGC 5364	91.4 ± 51.9	1	...	22.2 ± 8.9	22.2 ± 8.9	6,7,12	22.2 ± 8.9
NGC 5371	...	...	187.4 ± 13.3	175.7 ± 9.7	179.8 ± 7.8		179.8 ± 7.8
NGC 5377	...	...	118.1 ± 14.8	193.3 ± 10.0	169.7 ± 8.3		169.7 ± 8.3
NGC 5383	...	...	...	96.5 ± 8.7	96.5 ± 8.7	6	96.5 ± 8.7
NGC 5395	...	...	161.6 ± 13.2	135.5 ± 10.4	145.5 ± 8.2		145.5 ± 8.2
NGC 5448	...	...	121.4 ± 14.9	125.8 ± 9.7	124.5 ± 8.1		124.5 ± 8.1
NGC 5457	72.9 ± 16.6	1	...	23.6 ± 8.7	23.6 ± 8.7	7,8,12	23.6 ± 8.7
NGC 5473	221.6 ± 8.9	1	193.4 ± 15.6	233.3 ± 10.7	220.5 ± 8.8		220.5 ± 8.8
NGC 5474	...	...	...	29.0 ± 8.6	29.0 ± 8.6	7,8,12	29.0 ± 8.6
NGC 5485	159.1 ± 23.9	1	179.2 ± 14.6	221.8 ± 10.4	207.5 ± 8.5		207.5 ± 8.5
NGC 5523	...	...	...	30.1 ± 8.5	30.1 ± 8.5	6,7,12	30.1 ± 8.5
NGC 5548	291 ± 12	8	...	...	...	2	291 ± 12
NGC 5557	250.9 ± 12.1	1	283.2 ± 19.5	299.8 ± 11.9	295.3 ± 10.2		295.3 ± 10.2
NGC 5566	...	...	147.9 ± 11.8	167.0 ± 9.5	159.5 ± 7.4		159.5 ± 7.4
NGC 5576	182.3 ± 7.3	1	214.4 ± 17.9	218.2 ± 10.5	217.2 ± 9.1		182.3 ± 7.3
NGC 5585	42 ±	4	...	...	...	8,9	42 ±
NGC 5631	168.2 ± 10.8	1	173.6 ± 13.1	164.5 ± 10.5	168.1 ± 8.2		168.1 ± 8.2
NGC 5638	165.0 ± 3.5	1	142.0 ± 10.8	178.7 ± 9.8	162.1 ± 7.3		165.0 ± 3.5
NGC 5656	...	...	...	116.7 ± 9.0	116.7 ± 9.0	6	116.7 ± 9.0
NGC 5660	...	...	...	60.7 ± 9.4	60.7 ± 9.4	6	60.7 ± 9.4
NGC 5668	53 ±	4	...	...	...	6,9	53 ±
NGC 5669	...	...	...	...	...	1,2	32.4 ± 15.2
NGC 5676	117.8 ± 15.5	1	...	116.7 ± 8.9	116.7 ± 8.9	6	116.7 ± 8.9
NGC 5678	103 ±	4	...	132.8 ± 10.2	132.8 ± 10.2	6	132.8 ± 10.2
NGC 5690	...	...	...	...	...	1,2	<64.3
NGC 5701	115.2 ± 15.4	1	131.7 ± 11.6	119.2 ± 9.7	124.3 ± 7.4		124.3 ± 7.4
NGC 5746	182.5 ± 9.9	1	229.7 ± 15.1	187.4 ± 9.9	200.1 ± 8.3		200.1 ± 8.3
NGC 5775	...	...	120.0 ± 12.4	89.5 ± 9.2	100.3 ± 7.4		100.3 ± 7.4
NGC 5806	...	...	...	124.7 ± 9.1	124.7 ± 9.1	6	124.7 ± 9.1
NGC 5813	238.7 ± 4.8	1	232.9 ± 16.2	266.7 ± 11.3	255.6 ± 9.3		238.7 ± 4.8
NGC 5831	164.4 ± 4.7	1	161.4 ± 11.7	181.1 ± 9.7	173.1 ± 7.5		164.4 ± 4.7
NGC 5838	265.7 ± 9.3	1	268.7 ± 20.2	328.8 ± 12.6	312.0 ± 10.7		265.7 ± 9.3
NGC 5846	236.8 ± 4.4	1	225.3 ± 15.8	276.2 ± 10.3	261.0 ± 8.6		236.8 ± 4.4
NGC 5850	...	...	147.1 ± 10.5	135.4 ± 9.1	140.4 ± 6.9		140.4 ± 6.9
NGC 5866	158.9 ± 9.8	1	144.7 ± 13.7	181.8 ± 9.9	169.1 ± 8.0		169.1 ± 8.0
NGC 5879	73.9 ± 8.7	1	...	90.4 ± 8.9	90.4 ± 8.9	6	73.9 ± 8.7
NGC 5905	...	...	185.7 ± 25.0	172.9 ± 9.7	174.6 ± 9.0		174.6 ± 9.0
NGC 5907	...	...	108.7 ± 11.6	127.2 ± 9.0	120.2 ± 7.1		120.2 ± 7.1
NGC 5921	...	...	...	83.9 ± 9.2	83.9 ± 9.2	6	83.9 ± 9.2
NGC 5962	...	...	...	106.3 ± 9.5	106.3 ± 9.5	6	106.3 ± 9.5
NGC 5970	...	...	...	116.3 ± 9.0	116.3 ± 9.0	6	116.3 ± 9.0
NGC 5982	239.4 ± 5.2	1	272.4 ± 20.1	250.5 ± 11.0	255.5 ± 9.6		239.4 ± 5.2
NGC 5985	...	...	153.8 ± 12.3	159.8 ± 9.5	157.6 ± 7.5		157.6 ± 7.5
NGC 6015	...	...	...	43.5 ± 8.8	43.5 ± 8.8	6,7,12	43.5 ± 8.8
NGC 6070	...	...	...	93.7 ± 9.1	93.7 ± 9.1	6	93.7 ± 9.1
NGC 6140	34.4 ± 12.4	1	...	49.4 ± 8.9	49.4 ± 8.9	2	49.4 ± 8.9
NGC 6181	...	...	...	125.2 ± 9.0	125.2 ± 9.0	6	125.2 ± 9.0

Table 1
(Continued)

Galaxy	Literature		Palomar				Adopted
	σ (km s^{-1})	Reference	$\sigma_{\rm blue}$ (km s^{-1})	$\sigma_{\rm red}$ (km s^{-1})	$\sigma_{\rm final}$ (km s^{-1})	Notes	σ (km s^{-1})
NGC 6207	...	...	...	92.1 ± 10.0	92.1 ± 10.0	2	92.1 ± 10.0
NGC 6217	134.5 ± 19.6	1	...	70.3 ± 10.0	70.3 ± 10.0	8	70.3 ± 10.0
NGC 6236	...	...	...	...	...	1,2	46.1 ± 21.6
NGC 6340	143.9 ± 5.6	1	130.1 ± 10.5	147.9 ± 9.2	140.2 ± 6.9		143.9 ± 5.6
NGC 6384	124.3 ± 7.1	1	111.2 ± 10.9	135.4 ± 9.9	124.5 ± 7.3		124.3 ± 7.1
NGC 6412	29.8 ± 23.1	1	...	49.9 ± 9.0	49.9 ± 9.0	8	49.9 ± 9.0
NGC 6482	310.4 ± 11.5	1	...	337.0 ± 13.0	337.0 ± 13.0	8	310.4 ± 11.5
NGC 6500	214 ± 6	2	220.3 ± 17.1	212.0 ± 10.3	214.2 ± 8.8		214 ± 6
NGC 6501	215.9 ± 12.3	1	...	235.0 ± 10.7	235.0 ± 10.7	5	235.0 ± 10.7
NGC 6503	46 ± 3	2	...	...	...	5,7	46 ± 3
NGC 6643	72.3 ± 23.2	1	...	95.4 ± 9.2	95.4 ± 9.2	6	95.4 ± 9.2
NGC 6654	...	...	175.4 ± 12.3	170.2 ± 9.6	172.2 ± 7.6		172.2 ± 7.6
NGC 6689	26 ± 11	1	...	...	...	2,7	26 ± 11
NGC 6702	173.6 ± 4.9	1	...	169.6 ± 9.7	169.6 ± 9.7	5	173.6 ± 4.9
NGC 6703	179.9 ± 3.7	1	185.2 ± 13.4	191.4 ± 10.0	189.2 ± 8.0		179.9 ± 3.7
NGC 6946	...	...	...	55.8 ± 9.4	55.8 ± 9.4	2	55.8 ± 9.4
NGC 6951	97.9 ± 10.1	1	...	127.8 ± 9.1	127.8 ± 9.1	6	127.8 ± 9.1
NGC 7080	...	...	...	95.3 ± 9.4	95.3 ± 9.4	5	95.3 ± 9.4
NGC 7177	124.1 ± 3.7	1	128.8 ± 12.5	137.7 ± 9.2	134.6 ± 7.4		124.1 ± 3.7
NGC 7217	127.0 ± 10.1	1	155.0 ± 12.7	134.4 ± 9.1	141.4 ± 7.4		141.4 ± 7.4
NGC 7331	137.2 ± 3.5	1	144.3 ± 12.7	131.6 ± 9.1	135.9 ± 7.4		137.2 ± 3.5
NGC 7332	124.1 ± 3.5	1	131.3 ± 11.7	155.2 ± 9.4	145.8 ± 7.3		124.1 ± 3.5
NGC 7448	56.1 ± 14.8	1	...	77.6 ± 9.1	77.6 ± 9.1	6	77.6 ± 9.1
NGC 7457	69.4 ± 4.2	1	...	67.1 ± 8.5	67.1 ± 8.5	6	69.4 ± 4.2
NGC 7479	109 ± 11	1	151.6 ± 19.5	155.4 ± 9.4	154.7 ± 8.5		154.7 ± 8.5
NGC 7619	322.0 ± 5.8	1	315.9 ± 22.1	336.2 ± 12.7	331.2 ± 11.0		322.0 ± 5.8
NGC 7626	275.1 ± 5.2	1	262.4 ± 18.8	299.5 ± 11.9	288.9 ± 10.1		275.1 ± 5.2
NGC 7640	...	...	...	...	...	1,3,8	48.1 ± 22.5
NGC 7741	...	...	...	29.4 ± 8.9	29.4 ± 8.9	7,8,12	29.4 ± 8.9
NGC 7742	94.8 ± 11	1	...	73.3 ± 8.8	73.3 ± 8.8	8	73.3 ± 8.8
NGC 7743	83.8 ± 9.3	1	...	89.3 ± 9.1	89.3 ± 9.1	8	89.3 ± 9.1
NGC 7798	...	...	...	75.1 ± 9.2	75.1 ± 9.2	8	75.1 ± 9.2
NGC 7814	172.3 ± 7.7	1	191.9 ± 14.6	161.4 ± 9.5	170.5 ± 8.0		172.3 ± 7.7
NGC 7817	...	...	...	66.7 ± 8.4	66.7 ± 8.4	6	66.7 ± 8.4
UGC 3714	...	...	...	104.0 ± 9.4	104.0 ± 9.4	6	104.0 ± 9.4
UGC 3828	102.3 ± 25.1	1	...	73.9 ± 9.4	73.9 ± 9.4	6	73.9 ± 9.4
UGC 4028	...	...	...	80.5 ± 9.3	80.5 ± 9.3	6	80.5 ± 9.3
UGC 6484	...	...	...	61.1 ± 9.0	61.1 ± 9.0	6	61.1 ± 9.0

Notes. (1) The adopted velocity dispersion was estimated from the [N II] λ6583 emission line following the procedure of Ho (2009). (2) Stellar features too weak in the blue or red. (3) Spectrum partly corrupted. (4) The HyperLeda value of $\sigma = 240$ km s^{-1} pertains to the "southeast–northwest component of this merging galaxy; the correct dispersion for the primary nucleus is $\sigma = 100 \pm 25$ km s^{-1} (see Section 3.4). (5) Blue spectrum not available. (6) Blue spectrum not well resolved. (7) Red spectrum not well resolved. (8) Blue fit unreliable. (9) Red fit unreliable. (10) G band corrupted in blue; masked out. (11) The literature value corresponds to the central nuclear star cluster; the Palomar value is more representative of the central 2″×4″ region. (12) Velocity dispersion possibly overestimated slightly.

References. 1. HyperLeda; 2. Barth et al. (2002); 3. Kormendy & McClure (1993); 4. Ganda et al. (2006); 5. Wegner et al. (2003); 6. Batcheldor et al. (2005); 7. Héraudeau & Simien (1998); 8. Nelson et al. (2004); 9. Funes et al. (2002); 10. Sarzi et al. (2002); 11. Marconi et al. (2003); 12. Corsini et al. (2003); 13. Filippenko & Ho (2003).

(This table is also available in a machine-readable form in the online journal.)

the adopted value. Most of the literature values come from the HyperLeda database (Paturel et al. 2003), which, for any given galaxy, attempts to homogenize all published measurements into a single value by applying scaling factors determined from a set of "standard" galaxies measured through a roughly constant aperture size of 2″ × 4″. This aperture size, fortunately, exactly matches that employed in the Palomar survey.

For the final, adopted dispersion, there are strong reasons to prefer the Palomar measurements because of their homogeneity. Although in many cases their error bars formally exceed those of the literature sources, we believe that the error budget for the Palomar measurements is realistic, as evidenced, for example, from comparison with the high-accuracy measurements from Barth et al. (2002) for galaxies in common. Nevertheless, for concreteness, the final column of Table 1 lists either the final Palomar dispersion or the literature value, if available, based on whichever has the smaller formal error bar.

In total, our catalog gives new stellar velocity dispersion measurements for 428 galaxies, 88% of the parent survey. Of these, 142 (30%) have no previously published measurements. Not surprisingly, most of the new measurements are for late-type galaxies, systems where velocity dispersions are more

challenging to obtain because of their characteristically lower values ($\lesssim$100 km s^{-1}) and complications due to their composite stellar populations and contamination by emission lines. Our new measurements also provide updates to a number of literature dispersions that previously had large uncertainties or, in some instances, were grossly in error.

Stellar velocity dispersions could not be derived for 58 galaxies, mostly because their stellar features are too weak. For the sake of completeness, for the 34 of these objects that have emission lines, and for which no reliable dispersions exist in the literature, we list an indirect estimate of their stellar velocity dispersion based on their observed *gaseous* velocity dispersion derived from the line profile of [N II] λ6583. Using the current database, Ho (2009) finds that the kinematics of the ionized gas in the central few hundred parsecs of bulges generally trace the kinematics of the stars, such that $\sigma_g \approx (0.8\text{–}1.2)\sigma_*$. In detail, the normalization of the σ_g–σ_* relation shows a slight dependence on nuclear (Hα) luminosity and Eddington ratio, but *only* for sources spectroscopically classified as AGNs (LINERs, transition objects, and Seyferts). Those classified as H II (star-forming) nuclei obey $\sigma_g = 0.83\sigma_*$ with an rms scatter of 0.19 dex. This is the relation that we use because all of the 34 emission-line sources with very weak stellar features are H II nuclei (Ho et al. 1997a).[7] The error bars in the adopted dispersions come from the quadrature sum of the uncertainties in the original [N II] line widths (we conservatively assume 10%; Ho et al. 1997a) and the 0.19 dex scatter in the σ_g–σ_* relation.

5. SUMMARY

The Palomar spectroscopic survey has furnished considerable insights into the nature of nuclear activity in nearby galaxies (see Ho (2008) for a review). Aside from some considerations of the central stellar populations (Ho et al. 2003; Zhang et al. 2008), however, comparatively little analysis has been done on the absorption-line component of the spectra. This paper utilizes the survey spectra to derive a homogeneous set of new central stellar velocity dispersion measurements. A major obstacle is that the original survey data were not taken with this application in mind. In particular, neither the number nor the range of calibration template stars is ideally suited for deriving stellar velocity dispersions for galaxies with a wide range of composite stellar populations. The wavelength coverage of the blue-side and red-side spectra is nonstandard for velocity dispersion work and is rather sensitive to template mismatch. Moreover, the spectral resolution of the blue-side spectra is too coarse to yield reliable dispersions for most of the later-type galaxies in the sample.

We describe an effective strategy to address these challenges. We use the extensive Coudé-feed spectral library of Valdes et al. (2004) as the primary source of stellar templates. Applying a simple correction for the nominal relative resolution difference between the Valdes and Palomar systems yields velocity dispersions that show reasonably good agreement with literature values. The direct-pixel fitting code of Greene & Ho (2006) was adapted to solve for an optimally weighted linear combination of template stars, a crucial step to match the composite stellar population typically found in later-type galaxies. We demonstrate that the Ca+Fe λ6495 feature in the red-side spectra can be used to derive robust velocity dispersions, a crucial consideration because the resolution of the red setup, significantly higher than that of the blue setup, is sufficient to probe even the late-type systems in the survey.

Our final catalog lists a uniform set of new stellar velocity dispersions for 428 galaxies in the Palomar survey. A significant fraction of the galaxies, especially later-type systems, have no previously published velocity dispersions. Together with indirect estimates for another 34 objects and supplementary data from the literature, essentially all (482/486) of the galaxies in the Palomar survey now have central velocity dispersion measurements. The Palomar galaxies have been and continue to be heavily investigated for a variety of scientific applications. The catalog of velocity dispersions presented in this paper will add an important new dimension to the already rich database available for this much-studied galaxy sample.

We are very grateful to the staff of Palomar Observatory for their assistance with the observations over many years. We thank Aaron Barth and Dan Kelson for advice on methods of measuring velocity dispersions. An anonymous referee offered many helpful and critical comments that improved the paper. We acknowledge the usage of the HyperLeda database (http://leda.univ-lyon1.fr). The research of L.C.H. was supported by the Carnegie Institution of Washington. Support for J.E.G. was provided by NASA through Hubble Fellowship grant HF-01196, awarded by the Space Telescope Science Institute, which is operated by the Association of Universities for Research in Astronomy, Inc., for NASA, under contract NAS 5-26555. A.V.F. and W.L.W.S. are grateful for the financial support of the NSF, through grants AST-0607485 and AST-0606868, respectively.

[7] In detail, Ho (2009) notes that σ_g/σ_* for H II nuclei depends on σ_*, but for our present purposes we neglect this complication.

REFERENCES

Barth, A. J., Ho, L. C., & Sargent, W. L. W. 2002, AJ, 124, 2607
Batcheldor, D., et al. 2005, ApJS, 160, 76
Bender, R. 1990, A&A, 229, 441
Bernardi, M., et al. 2003, AJ, 125, 1817
Burbidge, E. M., Burbidge, G. R., & Fish, R. A. 1961, ApJ, 133, 393
Cappellari, M., & Emsellem, E. 2004, PASP, 116, 138
Corsini, E. M., Pizzella, A., Coccato, L., & Bertola, F. 2003, A&A, 408, 873
Davies, R. L., Burstein, D., Dressler, A., Faber, S. M., Lynden-Bell, D., Terlevich, R. J., & Wegner, G. 1987, ApJS, 64, 581
de Vaucouleurs, G., de Vaucouleurs, A., Corwin, Jr., H. G., Buta, R. J., Paturel, G., & Fouqué, R. 1991, Third Reference Catalogue of Bright Galaxies (New York: Springer)
Filippenko, A. V., & Ho, L. C. 2003, ApJ, 588, L13
Filippenko, A. V., Matheson, T., & Barth, A. J. 1995, ApJ, 455, L139
Filippenko, A. V., Matheson, T., Leonard, D. C., Barth, A. J., & Van Dyk, S. D. 1997, PASP, 109, 461
Filippenko, A. V., & Sargent, W. L. W. 1985, ApJS, 57, 503
Funes, J. G., Corsini, E. M., Cappellari, M., Pizzella, A., Vega Beltrán, J. C., & Bertola, F. 2002, A&A, 388, 50
Ganda, K., Falcón-Barroso, J., Peletier, R. F., Cappellari, M., Emsellem, E., McDermid, R. M., de Zeeuw, P. T., & Carollo, C. M. 2006, MNRAS, 367, 46
Graves, G. J., Faber, S. M., Schiavon, R. P., & Yan, R. 2007, ApJ, 671, 243
Greene, J. E., & Ho, L. C. 2006, ApJ, 641, 117
Héraudeau, Ph., & Simien, F. 1998, A&AS, 133, 317
Ho, L. C. 2008, ARA&A, 46, 475
Ho, L. C. 2009, ApJ, 699, 638
Ho, L. C., Filippenko, A. V., & Sargent, W. L. W. 1995, ApJS, 98, 477
Ho, L. C., Filippenko, A. V., & Sargent, W. L. W. 1997a, ApJS, 112, 315
Ho, L. C., Filippenko, A. V., & Sargent, W. L. W. 1997b, ApJ, 487, 568
Ho, L. C., Filippenko, A. V., & Sargent, W. L. W. 1997c, ApJ, 487, 579
Ho, L. C., Filippenko, A. V., & Sargent, W. L. W. 1997d, ApJ, 487, 591
Ho, L. C., Filippenko, A. V., & Sargent, W. L. W. 2003, ApJ, 583, 159
Ho, L. C., Filippenko, A. V., Sargent, W. L. W., & Peng, C. Y. 1997e, ApJS, 112, 391
Kelson, D. D., Illingworth, G. D., van Dokkum, P. G., & Franx, M. 2000, ApJ, 531, 159

Kormendy, J., & McClure, R. D. 1993, AJ, 105, 1793
Marconi, A., et al. 2003, ApJ, 586, 868
McElroy, D. B. 1995, ApJS, 100, 105
Minkowski, R. 1962, in IAU Symp. 15, Problems of Extra-Galactic Research, ed. G. C. McVittie (New York: Macmillan), 112
Morton, D. C., & Chevalier, R. 1972, ApJ, 174, 489
Nelson, C. H., Green, R. F., Bower, G., Gebhardt, K., & Weistrop, D. 2004, ApJ, 615, 652
Oke, J. B., & Gunn, J. E. 1982, PASP, 94, 586
Paturel, G., Petit, C., Prugniel, Ph., Theureau, G., Rousseau, J., Brouty, M., Dubois, P., & Cambrésy, L. 2003, A&A, 412, 45
Prochaska, L. C., Rose, J. A., & Schiavon, R. P. 2005, AJ, 130, 2666
Prugniel, Ph., Zasov, A., Busarello, G., & Simien, F. 1998, A&AS, 127, 117
Richstone, D. O., & Sargent, W. L. W. 1972, ApJ, 176, 91
Rix, H.-W., & White, S. D. M. 1992, MNRAS, 254, 389
Sandage, A. R., & Tammann, G. A. 1981, A Revised Shapley–Ames Catalog of Bright Galaxies (Washington, DC: Carnegie Inst. of Washington)
Sargent, W. L. W., Schechter, P. L., Boksenberg, A., & Shortridge, K. 1977, ApJ, 212, 326
Sarzi, M., et al. 2002, ApJ, 567, 237
Simkin, S. M. 1974, A&A, 31, 129
Stanford, S. A., & Balcells, M. 1990a, in IAU Colloq. 124, Paired and Interacting Galaxies, ed. J. W. Sulentic, W. C. Keel, & C. M. Telesco (Washington, DC: NASA Conference Publications No. 3098), 347
Stanford, S. A., & Balcells, M. 1990b, ApJ, 355, 59
Statler, T. S. 1995, AJ, 109, 1371
Tonry, J., & Davis, M. 1979, AJ, 84, 1511
Valdes, F., Gupta, R., Rose, J. A., Singh, H. P., & Bell, D. J. 2004, ApJS, 152, 251
van der Marel, R. P. 1994, ApJ, 270, 271
van der Marel, R. P., & Franx, M. 1993, ApJ, 407, 525
Wegner, G., et al. 2003, AJ, 126, 2268
Whitmore, B. C., McElroy, D. B., & Tonry, J. L. 1985, ApJS, 59, 1
Zhang, Y., Gu, Q.-S., & Ho, L. C. 2008, A&A, 487, 177